REVIEW PAPER

Methods to quantify primary plant cell wall mechanics

Amir J. Bidhendi[1,2,] ![ORCID] and **Anja Geitmann**[1,*,] ![ORCID]

[1] Department of Plant Science, McGill University, Macdonald Campus, 21111 Lakeshore, Ste-Anne-de-Bellevue, Québec H9X 3V9, Canada
[2] Institut de recherche en biologie végétale, Département de sciences biologiques, Université de Montréal, Montreal, Quebec H1X 2B2, Canada

* Correspondence: geitmann.aes@mcgill.ca

Abstract

The primary plant cell wall is a dynamically regulated composite material of multiple biopolymers that forms a scaffold enclosing the plant cells. The mechanochemical make-up of this polymer network regulates growth, morphogenesis, and stability at the cell and tissue scales. To understand the dynamics of cell wall mechanics, and how it correlates with cellular activities, several experimental frameworks have been deployed in recent years to quantify the mechanical properties of plant cells and tissues. Here we critically review the application of biomechanical tool sets pertinent to plant cell mechanics and outline some of their findings, relevance, and limitations. We also discuss methods that are less explored but hold great potential for the field, including multiscale *in silico* mechanical modeling that will enable a unified understanding of the mechanical behavior across the scales. Our overview reveals significant differences between the results of different mechanical testing techniques on plant material. Specifically, indentation techniques seem to consistently report lower values compared with tensile tests. Such differences may in part be due to inherent differences among the technical approaches and consequently the wall properties that they measure, and partly due to differences between experimental conditions.

Keywords: Acoustic microscopy, fracture, indentation, mechanical modeling, microfluidics, morphogenesis, multiscale models, plant cell mechanics, primary cell wall, tension test.

Introduction: the primary cell wall—a dynamic composite material

Plant cells are dynamic—they move, take shape, and act as force sensors and actuators, all without contractile protein–powered muscles (Geitmann, 2016; Bidhendi and Geitmann, 2018*a*). The remarkable features of plant cells and tissues have incited interest in recent years, not only among those studying plant morphogenesis and development but also among engineers and medical scientists who regard plants as smart materials (e.g. Luo *et al.*, 2015; Gershlak *et al.*, 2017; Zurlo and Truskinovsky, 2017) that can be utilized as scaffold (Gershlak *et al.*, 2017) or

inspire biomimetic design (e.g. Malik *et al.*, 2017). For all disciplines using plant material, a quantitative understanding of plant cell mechanics★ is essential [explanations of terms indicated with an asterisk can be found in the glossary (Table 4)]. The mechanical properties★ of plant cells and tissues depend largely on the apoplastic material—the cell wall and the middle lamella connecting cells.

Plant cell walls are built at the outer surface of the plasma membrane, either through exocytosis of structural

polysaccharides synthesized in the Golgi or directly by synthesis through plasma membrane-located enzymes. All plant cells form a thin primary wall that serves as a flexible envelope allowing the cells to grow. The secondary cell wall is generated during later developmental stages in certain cell types only. It is deposited between the existing primary cell wall and the plasma membrane, and usually appears after cessation of cell growth. Secondary walls govern the mechanics★ of sclerenchymatous tissues such as wood, for example, and therefore represent an attractive domain for biomechanical studies on resistance to external loads applied on tissues and organs. However, in this review, we focus on the application of cell mechanical methods on the primary cell wall that governs the developmental processes such as cell growth and morphogenesis.

The primary plant cell wall comprises cellulose microfibrils interacting with a matrix of mainly pectins, hemicelluloses, structural proteins, and water (Sandhu *et al.*, 2009; Bidhendi and Geitmann, 2016). During plant cell growth, this polymeric layer yields to and is stretched by the force driving this process—the turgor pressure★ and osmotically driven water influx. Growth regulation relies on spatiotemporal modulation of the mechanical behavior of the cell wall material, which in turn depends on the biochemical composition of the constituent polymers and the quality of linkages between them (Bidhendi and Geitmann, 2016; Cosgrove, 2018). A stiffening of cell wall material can, for example, be accomplished through the coordinated deposition of cellulose microfibrils either at selected subcellular regions or in a particular orientation, or both. Cellulose microfibrils are thought to be deposited and therefore reinforce the cell wall in the direction of maximal mechanical stresses★, in a process governed by the sensitivity of microtubules to stress fields (Hamant *et al.*, 2008; Landrein and Hamant, 2013). Such preferential orientation of cellulose microfibrils optimizes the design of this composite material to withstand stresses while minimizing the amount of building materials required to do so. We have recently reviewed the major cell wall constituents and their implication for plant cell wall mechanics and morphogenesis (Bidhendi and Geitmann, 2016).

While cell wall biochemistry is modulated to generate mechanical properties required for cell growth and function (for a review on Arabidopsis mutants with altered stiffness, see Brulé *et al.*, 2016), inversely, changes in the mechanical properties of the wall may also trigger cellular responses such as microtubule polymerization. Cell shape and local tissue topography affect the magnitude and orientation of stress fields in the cell wall (Bozorg *et al.*, 2014; Sampathkumar *et al.*, 2014; Echevin *et al.*, 2019; Kierzkowski and Routier-Kierzkowska, 2019). In a cell with cylindrical shape, for instance, the mechanical stress in the wall tends to be higher in the direction transverse to the long axis. This can promote the bundling of microtubules along the shorter axis. Under such a scenario, a closed feedback loop may result where cellulose deposition in the orientation of the stress field further reinforces the cell shape and growth anisotropy★. How the cell perceives its shape (Hamant and Moulia, 2016; Haupt and Minc, 2018) or the local stress or strain★ resulting from a particular shape is still poorly understood (Fruleux *et al.*, 2019). The flux of the plant hormone auxin seems to play a major role in mediating the signal (Heisler *et al.*, 2010; Hamant *et al.*, 2011; Nakayama *et al.*, 2012).

The mechanics of the cell wall plays a pivotal role in the regulatory mechanism governing plant cell morphogenesis and development. Several studies have revealed the mechanical properties of the plant cell wall to be intimately correlated with cell morphogenesis (Fayant *et al.*, 2010; Yanagisawa *et al.*, 2015; Amsbury *et al.*, 2016; Carter *et al.*, 2017; Majda *et al.*, 2017; Bidhendi and Geitmann, 2018*a*; Sapala *et al.*, 2018; Bidhendi *et al.*, 2019, Preprint). Quantitative approaches to investigate the mechanical behavior of the plant cell wall have, therefore, experienced considerable interest in recent years, and a surge of technological development has been dedicated to exploring plant cell mechanics. In this review, we summarize both conventional and emerging tools employed to address the need for experimental data pertaining to the mechanical characteristics of the primary plant cell wall; we elaborate on the challenges associated with each technique and provide suggestions. Many of the key mechanical and physical terminologies used in this text are already covered in excellent reviews, such as Boudaoud (2010), Milani *et al.* (2013), and Moulia (2013), to which we refer where appropriate. For the convenience of the reader, we also provide a glossary (Table 4) for terms marked with an asterisk in the text.

Study of plant cell mechanics requires tailored approaches

Experimental strategy in cell mechanics typically involves the application of a deforming force on the cell and measuring the cell's response to that force. The deformations★ can be in the form of stretching, compression, bending, or shear of the material (see stress★ and strain★). Because of the presence of the cell wall, some of the technical tools used for mammalian cells seem challenging if not impossible to use for plant cells. For instance, micropipette aspiration or magnetic twisting, while widely used to determine viscoelastic★ properties of mammalian cells (Lim *et al.*, 2006; Bidhendi and Korhonen, 2012), have not been used so far for assessing plant cell mechanics. This is due either to technical difficulties or to the inability to produce forces strong enough to act against the cell wall and the turgor pressure. These techniques may be used to investigate plant protoplasts, however. Another difference between mammalian and walled cells arises from the wall's macromolecular structure. While mammalian cells can exhibit anisotropy due to a preferential arrangement of cytoskeletal stress fibers (Hu *et al.*, 2004), typically, their mechanics, while heterogeneous, is idealized as isotropic. In walled cells, anisotropy is an essential feature on the other hand, especially in elongating cells. Combined with subcellular heterogeneity, anisotropy determines the growth pattern of the individual cell (Baskin, 2005; Cosgrove, 2005; Sanati Nezhad and Geitmann, 2015; Bidhendi and Geitmann, 2016). Both parameters, therefore, need to be considered when evaluating plant cell mechanics, and the methods need to be tailored for these features.

Scratching below the surface: indentation techniques in plant cell mechanics

Indentation-based methods have been widely used to study the mechanics of animal (Alcaraz *et al.*, 2003; Li *et al.*, 2008) and plant cells and tissues (Zerzour *et al.*, 2009; Peaucelle *et al.*, 2011, 2015; Fernandes *et al.*, 2012; Radotić *et al.*, 2012; Routier-Kierzkowska *et al.*, 2012; Forouzesh *et al.*, 2013; Bou Daher *et al.*, 2018). These techniques use a rigid probe either to induce a local deformation on the specimen while measuring the reaction forces or to apply a defined force while measuring the deformation of the sample (Fig. 1A). The resulting force–indentation curve can be used to derive several mechanical parameters including, but not limited to, the indentation modulus★ (or apparent modulus, related to elastic moduli★), as well as plastic★ and viscoelastic properties of the specimen. Several models are available that are widely used to infer the apparent Young's★ modulus (an elastic modulus★) of the sample from the loading–unloading curves, such as variations of the Hertz model or use of inverse finite element analysis. Whether the indentation (loading) or retraction (unloading) portion of the loading–unloading curve is used to assess the behavior of the material depends on considerations specific to the experimental set-up such as radius of the probing tip or presence of adhesive forces on the surface of the sample. While the retraction curve is sometimes chosen to calculate the indentation modulus to exclude the plastic deformations, the indentation curve is sometimes preferable to avoid the effect of adhesion★ forces that may become significant during retraction (Peaucelle *et al.*, 2015; Bou Daher *et al.*, 2018). Viscoelastic properties are measured by dynamic indentation (see dynamic analysis★) resulting in the identification of complex moduli★ that hold information on both elastic and viscous★ properties of the cell wall in the frequency domain. Relaxation★ or creep★ tests are also possible by keeping the load or indentation depth constant and measuring the subsequent changes in indentation depth or force, respectively. Several excellent reviews describe the fundamentals of indentation techniques in probing the mechanics of biological matter including plant cells (Butt *et al.*, 2005; Kuznetsova *et al.*, 2007; Kirmizis and Logothetidis, 2010; Milani *et al.*, 2013; Routier-Kierzkowska and Smith, 2013; Guz *et al.*, 2014; Haase and Pelling, 2015; Maver *et al.*, 2016).

Indentation techniques allow for excellent spatial and force resolution, and minimal sample preparation facilitates *in vivo* studies. Indentation set-ups range greatly from nanoindentation using instrumented nanoindenters, to the versatile use of atomic force microscopy (AFM) and variations of microindentation systems (Cretin and Sthal, 1993; Routier-Kierzkowska *et al.*, 2012). A wide spectrum of sophistication, resolution, and application exists among the indentation systems with the possibility of measuring forces in the range of picoNewtons and spatial (lateral and vertical) resolution close to Ångströms. Indentation methods differ in the size and shape of the probing tips, depth of deformation, or magnitude of measured forces. In many indentation systems, the rigid probing tip that comes into contact with the sample is attached to a deformable cantilever that bends upon contact of the probe with the sample. In conventional AFM systems, changes in the position of the laser reflected off the surface of the cantilever on a photodetector are used to measure the deformation of the cantilever due to contact of the rigid probe with or its proximity to the sample surface (Fig. 1B). There are several different types of cantilever deflection, including vertical bending, lateral bending, and torsion★. In contact, non-contact, and tapping modes of AFM the vertical bending mode is dominant, while in some other applications such as torsional resonance mode or lateral force microscopy (LFM), the other cantilever deformation modes become significant (Song and Bhushan, 2006). The bending of the cantilever, which has a known spring constant, allows for quantification of the force deforming the sample. The spring constant of the cantilevers is, therefore, an important parameter of the experimental set-up, and choosing it requires an educated guess of the sample's stiffness★. The cantilever should be flexible enough to be deformed by the contact with the sample, but strong enough to deform the sample. In other words, as with any detection system, the dynamic range of the cantilever has to fit the magnitude of the stiffness of the sample. While manufactured cantilevers come with a 'nominal' spring constant, researchers often calibrate the spring constant independently. Among common ways to this end are thermal tuning (Levy and Maaloum, 2001) and indentation on a standard sample of known stiffness generally provided by the manufacturer. A considerable variation of probing tips exists in terms of shape, size, and aspect ratio (Fig. 1C). Knowledge of the tip geometry is crucial in the analysis of test results as it directly determines the contact surface between the tip and the sample. While tip shape parameters are often provided by the manufacturers, exact shapes warrant independent validation. Even if that is done prior to an experiment series, wear and tear of the fine tips during scanning and contact with the sample can significantly alter their features, an effect that needs to be considered. When a tipless cantilever or a flat indenter is used with a size similar to or larger than the dimension of the cell, the method is termed cell compression. This approach has been used for tomato cells (Wang *et al.*, 2004) and plant cell protoplasts (Durand-Smet *et al.*, 2014), allowing for the calculation of elastic and time-dependent properties of these cells.

Indentation techniques have contributed significantly to our understanding of primary plant cell wall mechanics and cell growth in the past decade. Marga *et al.* (2005) used AFM indentation combined with SEM to investigate how expansin proteins affect cell wall creep and growth. Microindentation revealed a significant correlation between the configurational changes in the cell wall polymer pectin and the cell wall mechanics associated with polar and oscillating growth in pollen tubes (Parre and Geitmann, 2005; Zerzour *et al.*, 2009). Combining fluorescence microscopy and nanoindentation using AFM, Milani *et al.* (2014) correlated the alterations in stiffness of shoot apex cells in *Arabidopsis thaliana* to gene expression. Peaucelle *et al.* (2015) used AFM indentation to investigate changes in pectin and cellulose orientation related to mechanical and growth symmetry breaking in hypocotyl epidermal cells, revealing a role for pectin demethylation in cell growth regulation. Yakubov *et al.* (2016) used AFM to reveal
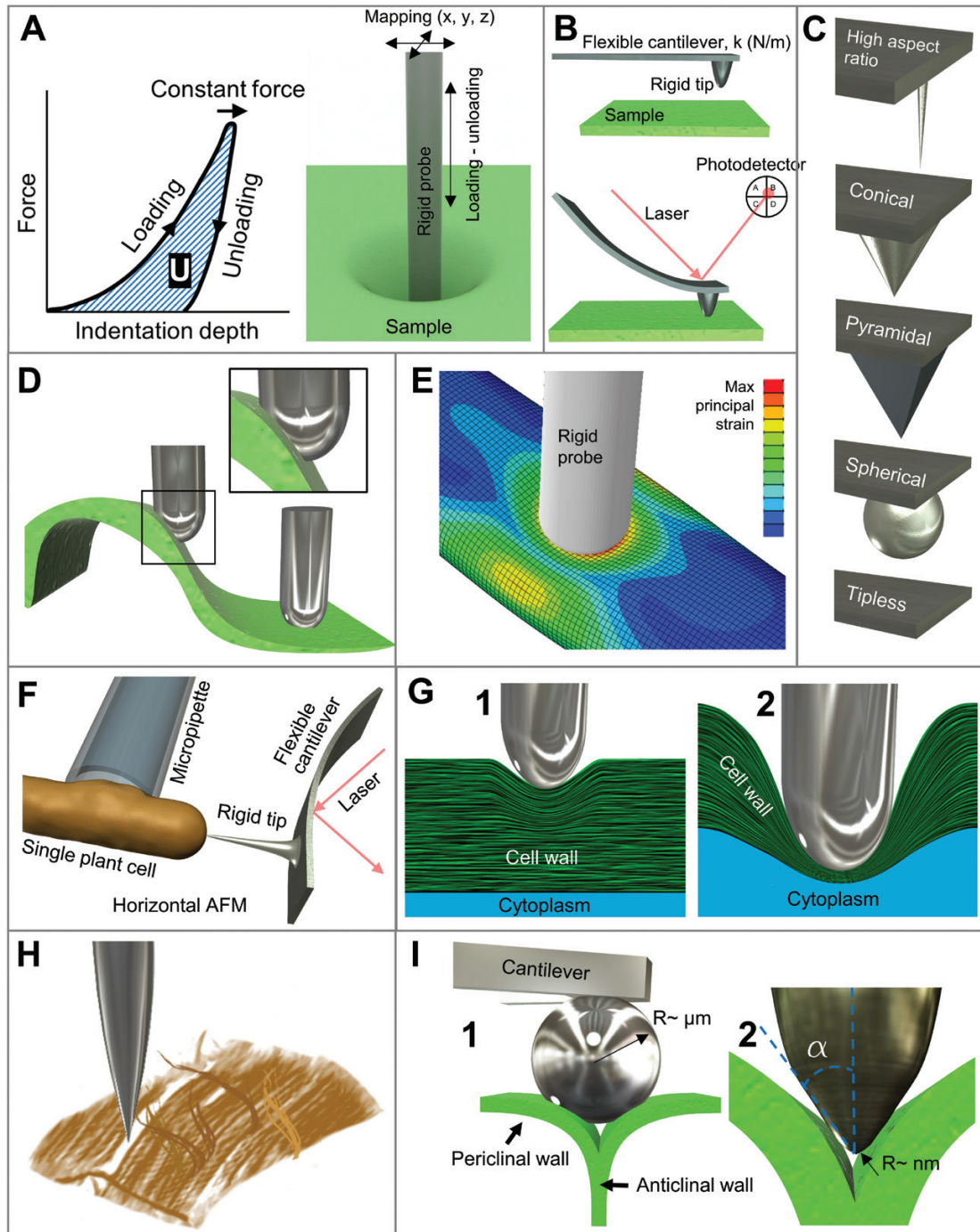
Fig. 1. (A) Schematic of a typical indentation experiment with loading, constant force (holding), and unloading segments of the force–indentation trace. Different paths of loading–unloading mark energy dissipation (U) due to internal friction in the material. Surface rastering and indentation/force sensing directions are perpendicular to each other. (B) Force measurement and topographical imaging in a typical cantilever-based indentation system as in common AFMs. Forces arising due to proximity of or contact between the rigid tip and the sample result in the bending of the flexible cantilever. Changes in direction of the laser beam reflected off the surface of the cantilever allow measurement of forces, based on the bending of the cantilever of a known spring constant (k). (C) Great variability exists between indenter tip geometries, sizes, and aspect ratios. Size and geometry of tips affect the force measurement and topographical imaging artifacts. (D) Tip geometry and curvature of the specimen influence the contact quality and therefore the measured forces. (E) Finite element model of indentation of a hollow elastic cylinder with a rigid probe. The heatmap shows the maximum principal strain field. Shape and aspect ratio of the sample affect the contact, and consequently the stress and strain fields under indentation. In this case, an elliptical deformation pattern can be observed, although the material is isotropic, and the probe cross-section is flat and circular. (F) Horizontal AFM set-up to probe perpendicularly to the highly curved regions of a single plant cell. The cell may be immobilized by exertion of a negative pressure via a micropipette. (G) The depth of the indentation determines to what extent the inner layers of a single wall and the turgor pressure contribute to the measured forces. (H) Fibers may move apart in indentation using a sharp probe. This has the potential to alter the measured stiffness, for instance by measuring predominantly the pectin-rich matrix instead of the overall wall properties. (I) Effect of fine topographical features of the cell such as cell borders. With a (1) large probe, the probing tip of the indenter may not come into contact with the cell border, and access deep trenches. Further, the deformation may not be limited only to the target structure being investigated. (2) A sharper probe tip enables studying the finer cellular features. In either case, the tip of the probe may or may not reach the deep valleys between the cells. Reinforcement by vertical anticlinal walls may contribute to the 'sensed' stiffness.

a heterogeneous distribution of stiffness in the primary cell wall of suspension-cultured cells of *Lolium multiflorum* and leaf epidermal cells of *A. thaliana*. Besides the characterization of local mechanical properties, indentation techniques allow for imaging and mapping of the surface topography—a major application of AFM since its invention. In recent studies, this aspect of AFM has been employed to visualize the orientation of cellulose microfibrils. In such an approach, cellulose microfibrils must be exposed in order to be accessible to the indenter. This requires partial removal of the cuticle and matrix materials such as pectin to expose the cellulose, although, reportedly, one study seemed successful in imaging the cellulose orientation in intact untreated outer cell wall surfaces of cotyledons (Sampathkumar *et al.*, 2014). Alternatively, the inner face of the wall (closest to the plasma membrane) is probed after breaking the cells open, although this approach is destructive (Zhang *et al.*, 2014; Xi *et al.*, 2015; Zhang *et al.*, 2016). The inner face of the cell wall features the newest wall layer that often exhibits an orientation of cellulose microfibrils that is predominantly transverse to the growth axis and has been proposed by some studies to be the most influential layer of the cell wall in determining the cell elongation (e.g. Richmond *et al.*, 1980). Whether this correlation truly indicates causality warrants further study, but, while the different wall layers may have different orientation of cellulose microfibrils, and experience different degrees of stress, the effective stiffness and deformability of the overall wall structure is probably a superposition of all layers. Despite the growing number of indentation-based studies, protocols for reproducible results and absolute values for relevant mechanical parameters of the cell wall remain challenging. Cell wall curvature, such as of the outer periclinal★ walls of the epidermis, can influence the indentation outcome. In those configurations of the indentation systems that rely on vertical force measurements, it is the vertical projection of surface reaction forces that align with the axis of the indenter tip that is effectively measured (Routier-Kierzkowska and Smith, 2013). At non-normal contact angles, other parameters such as friction become apparent which influence the measured force (Fig. 1D). To what degree the oblique contact affects the force measurement is determined by tip shape parameters such as radius and opening angle (for non-spherical tips). Any oblique application of forces may also induce other types of deformation such as in-plane strain and shear, confounding the outcome. The significance of these effects needs to be evaluated separately. Evaluation of the influence of surface topography and roughness and correction of indentation measurements is the subject of ongoing research (Mazeran *et al.*, 2005; Heinze *et al.*, 2018). The oblique contact has been reported to be associated with both underestimation and overestimation of the measured value of stiffness. A possible way to avoid such geometrical complications is to keep the indenter perpendicular to the surface, which, however, would require a system that can rotate the tip or the sample to ensure that the tip is oriented at the normal axis of the specimen at all subcellular locations. Available systems do not allow for such flexibility. To circumvent this issue, many studies choose regions of interest from relatively flat sections of tissue and cells (Peaucelle *et al.*, 2015).

Besides the curvature of the outward-facing cell wall, the dimensions and the aspect ratio of the cell can also result in uneven indenter–sample contact, reflected in the stress and strain fields as well as the modulus obtained through indentation (geometrical stiffness★ compared with material stiffness). For instance, the indentation of a longitudinal object (hollow cylinder consisting of an isotropic★ material, Fig. 1E) by a cylindrical rigid tip with circular cross-section causes a strain pattern around the indentation surface that is elliptical rather than circular, due to geometrical, rather than material, features. Several papers have discussed the discrepancies arising due to the tip–sample contact angle (Routier-Kierzkowska *et al.*, 2012; Braybrook and Peaucelle, 2013; Milani *et al.*, 2013; Mosca *et al.*, 2017), and additional studies are warranted to overcome the tip–sample angle and geometry problems. We surmise that a strategy to acquire more information from the indentation experiments on plant cells would be to measure lateral forces in conjunction with the force obtained from vertical indentations. LFM is a special application of AFM commonly used in nanotribology to study the frictional forces in materials with varying surface properties. In LFM, the tip moves parallel to the surface, providing a measure of in-plane elasticity of the sample (Perry, 2004). While powerful, the relevance of this approach for the mechanics of the plant cell wall is yet to be evaluated. Combining perpendicular and lateral scanning modes may prove beneficial in studies of plant cells commonly exhibiting highly curved profiles. This is specifically crucial for cases where the mechanics of the highly curved region is of particular interest, such as in tip-growing cells. In such cases, a horizontal AFM set-up, a 90° rotation of a conventional AFM, may be used to probe perpendicular to the region of interest, similar to the set-up reported by Ounkomol *et al.* (2009). In such a scenario, the cell has to be held in place laterally, which can be done using a micropipette (Fig. 1F) or a perpendicular flow (Sanati Nezhad *et al.*, 2013b) in a compartmentalized microfluidic device.

Another consideration for indentation-based measurement of plant cell mechanics is the determination of the appropriate indentation depth (Han *et al.*, 2016). In shallow indentations, the properties of the cuticle or the wall layers directly below the tip may dominate the results (Fig. 1G). Given that these outer layers may structurally differ from the inner cell wall layers, for instance in cellulose orientation, extrapolation from outer wall measurements is inherently associated with simplifying assumptions for the 3D structure of the cell wall. In deeper indentations approaching the thickness of the cell wall, the contribution of the turgor pressure and the support substrate cannot be ignored (Yakubov *et al.*, 2016). Several studies have taken advantage of this fact in solving a system of equations with two variables to obtain both the cell wall stiffness and the turgor pressure. This is carried out either by combining data from varying indentations depths (Forouzesh *et al.*, 2013) or by combining deep indentations with osmotic treatments (Beauzamy *et al.*, 2015; Weber *et al.*, 2015). Indentation methods provide a minimally invasive means to measure the turgor pressure and have been shown to produce values similar to those obtained by other techniques such as pressure probe

(Green, 1968; Wang *et al.*, 2006) and ball tonometry (Lintilhac *et al.*, 2000; Wei *et al.*, 2001). Similarly, squeezing the plant cell between two parallel microplates, considering a thin pressurized shell behavior for the cell, has been used to estimate the turgor (Durand–Smet *et al.*, 2017). Computational modeling has been used to determine two or more unknowns from single indentation experiments, such as Young's modulus★ and Poisson's ratio★ (Zheng *et al.*, 2009).

While indentation produces absolute values for mechanical parameters, these may not necessarily be relevant for the biological phenomenon investigated. For example, it remains unexplored to what degree the modulus acquired by the out-of-plane indentation of a cell corresponds to in–plane properties of the cell wall. Deformation of the cell wall during indentation is a combination of cell wall compression and bending (Fig. 1G). While the bending component is correlated with the in–plane elastic modulus of the wall, the compression of the wall is related to its compliance★ through its thickness (Yakubov *et al.*, 2016). Indeed, a finite element analysis by Milani *et al.* suggests that the deformation of indentation may be considerably more sensitive to the elastic modulus of the wall in the direction of its thickness (normal to the in–plane direction) rather than its in–plane properties (supporting information Milani *et al.*, 2011). However, even if the measured indentation modulus relates to the in–plane properties, it may not directly correlate with the cell wall properties pertinent to plant cell growth, due to the anisotropic★ nature of cell walls. The modulus measured by indentation of the anisotropic material is commonly thought to be an average of stiffness in different directions (Vlassak and Nix, 1994; Vlassak *et al.*, 2003; Eder *et al.*, 2013). Therefore, the data acquired by indentation techniques must be reconciled with the in–plane tensile properties of the plant cell wall, and some degree of directional information must be incorporated. It remains to be verified whether indentation can distinguish changes in cell wall anisotropy if the average cell wall stiffness was unaffected. Tanguy *et al.* (2016) measured the elastic modulus of plant fibers used to reinforce composite materials, and compared the values obtained by indentation using a nanoindenter and tensile testing methods. The results obtained for various fibers such as sisal and Eden flax fibers indicated a considerable underestimation of the elastic modulus of the samples when measured by indentation compared with tensile testing. These results suggest that the indentation modulus may differ greatly from the elastic modulus of the cell wall corresponding to the in–plane resistance against tension along the main orientation of the fibers. Comparison between the indentation and tensile moduli of plant samples with primary cell wall confirm this as, typically, indentation seems to yield considerably lower modulus values compared with tensile tests (Tables 1, 2). This begs for caution using indentation techniques for evaluation of strongly anisotropic materials such as plant cell walls. Tanguy *et al.* (2016) suggest that by pushing the nanoindenter into the sample, the microfibrils can slightly separate (Fig. 1H), a potential source of discrepancy between the indentation and tensile tests in addition to other factors. While the authors tried to establish a relationship between the nanoindentation and tensile estimated values for elasticity, it was suggested that such a ratio might vary from tissue to tissue due to variations in fiber angles. The higher the anisotropy, the larger the difference between the outcome of tensile tests and nanoindentation. However, by application of a correction coefficient, reasonable estimates could be found. This is useful when other techniques such as tensile testing are difficult to perform, for example because of the miniature size of the sample. In a different approach, Nakamura and Gu (2007) used two indenter tip geometries to induce different strain fields. This allowed acquiring more data from their samples, thermally sprayed coatings with transversely isotropic properties (refer to elastic modulus in Table 4). The authors used an inverse search method to obtain the elastic properties of the thin films along the two perpendicular material axes. Similar strategies may be promising in the investigation of plant cell wall anisotropy. Several studies have discussed the theoretical and experimental basis of anisotropic indentation providing the potential frameworks for adaptation to the anisotropic walls of growing plant cells (refer to Vlassak and Nix, 1994; Jäger *et al.*, 2011). Combining indentation measurements with monitoring the wall strain pattern, by using fluorescent markers (for instance refer to Kim *et al.*, 2015), may be an alternative to obtain an estimate of the material anisotropy.

Besides cell wall topography and curvature, the geometrical features of plant cells and tissues can affect the measurements obtained by indentation. Rather than blocks of solid material, plant cells resemble fluid-filled boxes with periclinal★ walls and anticlinal★ walls defining the cell boundaries. Published stiffness maps of epidermal tissues have reported elevated stiffness values at the anticlinal walls and near the tricellular junctions (Peaucelle *et al.*, 2015; Carter *et al.*, 2017). When interpreting stiffness maps of tissues, a first concern is whether the probe tip actually comes into contact with the anticlinal walls or remains in contact with parts of the periclinal walls. This arises from the geometrical features of the tissue. With larger probing tips, such as spherical types with radii in the micrometer range, the indenter tip may not reach directly above the anticlinal wall (Fig. 1I1) and instead pushes on a region comprising both periclinal and anticlinal wall. While this indentation can still be insightful, the measured properties cannot be interpreted to directly refer to the anticlinal wall. Even with finer tip radii, the tip may still not come into contact with the anticlinal walls due to factors such as the shape of the tip or its opening angle (Fig. 1I2). Bulging of the periclinal walls can exacerbate the issue by forming deep trenches at the cell borders. The use of plasmolyzed tissues aims at circumventing this challenge by deflating the periclinal walls (Peaucelle *et al.*, 2015; Carter *et al.*, 2017). Cell and tissue topographical maps acquired simultaneously with stiffness maps during indentation tests can provide important validation for such evaluations. Secondly, regardless of whether or not the probe comes into contact with the anticlinal wall, the measured values in regions of cells containing the anticlinal walls are likely to reflect, to some degree, the stiffness due to the presence of vertically arranged anticlinal walls supporting the periclinal walls at this location (Fig. 1I). In other words, rather than measuring the material properties of the outer wall, the indentation might measure the geometrical stiffness of the 3D structure, similar to the effect proposed by Mosca *et al.* (2017) for microindentation. This question arose

Table 1. *Indentation modulus (IM) for various plant cell types (updated versions of this table can be found at:* www.plantbiomechanics.net/databases)

Publication	IM (MPa)	Cell/tissue	Turgidity	Cantilever stiffness (N m⁻¹)	Tip R (nm), shape	Additional notes
Yakubov *et al.* (2016)	0.03–0.09	Pavement cell/abaxial leaf epidermis AT, 3 weeks post-germination	Turgid[†]	1–10	Various, R<10 and ~20, conical[††]	Max force (nN):100–1000, speed (nm s⁻¹): 200–1000. Values taken from fig. 10 of the publication. [†]Turgidity: leaf samples were from plants in Petri dishes. Measurements were performed in air. [††]Shape of tip taken from fig. 3 of the publication.
Sampathkumar *et al.* (2014)	2–8	Pavement (and guard) cells/abaxial cotyledon epidermis AT, 5 d post-germination	Turgid	0.3–0.5	2–10, pyramidal	Max force (nN): 1000, speed: oscillation frequency is given as 0.5 kHz (0.002 s for a loading–unloading cycle). The linear indentation speed could be calculated based on peak indentation amplitude and the period of time. Measurements were carried out under water.
Carter *et al.* (2017)	~5–60	Guard (and pavement) cells/adaxial leaf epidermis AT, 3–4 weeks old	Plasmolyzed	45	5, pyramidal	Max force (nN): 1000, max indentation (nm): 100–1000. Stiffness values showed sensitivity to cellulase application. A gradient of stiffness was observed over the periphery of the mature but not immature guard cells, which is proposed as a mechanical factor underlying stomatal pore opening.
Forouzesh *et al.* (2013)	~80–160	Pavement (and guard) cells/abaxial leaf epidermis AT, 12–52 d old	Turgid and plasmolyzed	N/A[†]	2500, spherical	Max force (nN): 25 000[††], max indentation (nm): 1800, varying indentation depths, speed (nm s⁻¹): 200. The indentation modulus computed for the cell wall was sensitive to the turgor pressure. Interestingly cell wall of turgid samples kept in water were reported to be less stiff than control (air) or plasmolyzed samples upon unraveling the cell wall stiffness and turgor pressure. [†]Cantilever-less system; an instrumented nanoindenter was used. [††]Max force and indentation depth are obtained from fig. 1 of the publication.
Beauzamy *et al.* (2015)	~1–12	Pavement cells/outer face of outer periclinal wall of adaxial onion epidermis	Turgid and plasmolyzed	42	400, spherical	Max force (nN): 10 000, max indentation (nm): 1000 (turgid cells) and 8000 (flaccid cells), speed (nm s⁻¹): 10 000. A method was developed to extract turgor pressure and cell wall stiffness from in-dentation tests. Turgor pressure was found to be influential in the apparent stiffness, probably due to deeper indentations.
Xi *et al.* (2015) and Tittmann and Xi (2014)	~6–22	Pavement cells/inner face of outer	Hydrated	0.7	Unknown, pyramidal	Max force (nN): 15, max indentation (nm): 150, speed (nm s⁻¹): 800. Since the inner periclinal walls are usually removed during detachment of the abaxial onion epidermis, the cells are broken, and turgor pressure is removed. Application of EDTA decreased the cell wall elastic modulus. In contrast, addition of $CaCl_2$ increased it.
Yakubov *et al.* (2016)	0.01–10 (mean 0.7)	Suspension-cultured cells/starchy endosperm, *Lolium multiflorum*	Turgid and plasmolyzed	0.05–1	Various, R<10 and ~20, conical[†]	Max force (nN): 500, max indentation (nm): 500, speed (nm s⁻¹): 200–1000. It was noted that cell wall stiffness values can vary several orders of magnitude at the subcellular scale. In other words, very local properties can vary greatly from average values for the cell wall. Turgor pressure was deemed influential in indentations approaching wall thickness. [†]Shape of tip taken from fig. 3 of the publication.
Radotić *et al.* (2012)	0.1–1	Suspension-cultured cells/AT, 4–20 d of	Turgid	0.06	20, unknown	Max force (nN): 1.4, indentation (nm): varying indentation depths <80 nm. Unexpectedly, the cell walls appeared less stiff in the first and final phases of cell growth than during the exponential growth phase.

Table 1. *Continued*

Publication	IM (MPa)	Cell/tissue	Turgidity	Cantilever stiffness (N m⁻¹)	Tip R (nm), shape	Additional notes
Peaucelle *et al.* (2015)	0.1–0.4	Epidermal cells/dark grown hypocotyl, AT, ≤24 h post-germination	Plasmolyzed	1.5 (estimated, nominal values were between 10 and 130, article's supplementary information)	900–1100, spherical	Indentation assay is based on the protocol from Peaucelle *et al.* (2011). Transverse anticlinal walls appear stiffer than longitudinal anticlinal (and periclinal) walls. Anticlinal wall stiffness was correlated with growth anisotropy. Measurements were shown to be sensitive to interference with pectin. Anticlinal walls of hypocotyl epidermal cells in PMEI3oe overexpression line, PMEI3oe, appeared stiffer than those of wild-type Arabidopsis, which, in turn, appeared stiffer than anticlinal walls in PME5oe line.
Bou Daher *et al.* (2018)	10–50	Epidermal cells/dark-grown hypocotyl, AT, ≤48 h post-germination	Plasmolyzed	45	5, pyramidal	Max force (nN): 500, max indentation (nm): 250–500, speed (nm s⁻¹): 100 000 (from the published protocol on AFM elastography of plants Braybrook, 2015) Differences in stiffness between anticlinal walls in non-transgenic and pectin mutants were detected. Same as in Peaucelle *et al.* (2015), wall length and its stiffness seemed to be correlated linearly (fig. 3-figure supplement 1). The longer walls of epidermal cells appeared consistently softer than shorter walls. This included not only the axial (in direction of hypocotyl axis) walls appearing softer than transverse walls, but also each of the transverse and longitudinal walls appearing progressively softer as cells grew and expanded.
Peaucelle *et al.* (2011)	0.1–0.6	L1 layer cells (with contribution from underlying layers)/shoot apical meristem, AT	Plasmolyzed	0.52 (for probes with 5000 nm radius bead) and 10–130 (for probes with 900–1100 nm radius tip or tipless probes)	900–1100, 5000, spherical	Max force (nN): ~30 (modulated to obtain a constant indentation depth), max indentation (nm): ~30, speed (nm s⁻¹): 3330 (calculated based on constant 500 nm indentation depth in 0.3 s accounting for both approach and retraction). Changes in indentation modulus were detected related to organ initiation and pectin chemistry in primordia. Different indentation depths were used to distinguish changes in epidermis and underlying layers.
Braybrook and Peaucelle (2013)	0.05–0.5	L1 layer cells (with contribution from underlying layers)/shoot apical meristem, AT	Plasmolyzed	1.5 (estimated for those used, 10–130 nominal values)	900–1100, 5000, spherical	Max indentation (nm): 250–500, indentation assay is based on the protocol from Peaucelle *et al.* (2011). Smaller values of indentation modulus were obtained with smaller tip radius (e.g. ~0.06 MPa compared with ~0.4 MPa). Changes in cell wall elasticity could be linked with application of auxin and changes in pectin chemistry.
Milani *et al.* (2011)	1.5–5	L1 layer cells at the tip and flank/shoot apical meristem, AT	Turgid and plasmolyzed	0.16	10–40, pyramidal	Max indentation (nm): 100 Tip of the shoot apical meristem was found to appear stiffer (~5±2 MPa) than the peripheral region (~1.5±0.7 MPa). Plasmolysis was performed to rule out a significant contribution from turgor on measurement of wall stiffness.
Burri *et al.* (2019)	11±4	Pollen tube/lily	Turgid	72 (240 for cell compression)	400, spherical	Max indentation (nm): >2000 (fig. 2D of Burri *et al.*, 2019). Thickness of the wall was taken from literature as 190 nm, which allowed estimation of average Young's modulus. Cell compression was also performed on cells.
Vogler *et al.* (2013)	20–90	Pollen tube/lily	Turgid and plasmolyzed	N/A	400, spherical	Max force (nN): 3500, max indentation (nm): 300–400. Turgor pressure and Young's modulus were estimated based on cell wall thickness.

AT: *Arabidopsis thaliana*

in a study by Peaucelle *et al.* (2015) that found that shorter anticlinal wall segments were stiffer under indentation than longer ones. A similar observation was made by Bou Daher *et al.* (2018) which is consistent with the flexural★ behavior of beams of different lengths or shape of cross-section. However, the appearance of the stiffness differential preceding the apparent changes in cell geometry was used to support the hypothesis that the difference in apparent stiffness of the cell walls was caused by biochemical changes in those walls and not their geometry (supplemental information Peaucelle *et al.*, 2015). Such a rationale is further supported by an earlier study by Milani *et al.* (2011) using a different AFM indentation set-up in terms of tip radius and indentation depth and on a different tissue (see Table 1) where central regions of the outer periclinal walls of shoot apical meristem cells were not found to be softer than spots near the cell borders. This is interesting since, at least for Arabidopsis leaf pavement cells, the central regions of cell walls are suggested to be thinner than the regions close to the anticlinal walls (Forouzesh *et al.*, 2013).

Table 1 provides a list of indentation moduli from a few recent studies on plant cells and summarizes the testing conditions such as depth of indentation and state of turgidity of the measured cells. It can be observed that the indentation moduli found for plant cells walls in these studies vary by more than four orders of magnitude, even for the same cell types of the same plant species. Considerable variations were also observed in some of the testing parameters such as tip shapes and tip radius values, as well as the cantilever stiffness, which varies between very soft (0.01 N m^{-1}) to intermediately stiff (~50 N m^{-1}). The differences may be compounded by different loading–unloading velocities, and the analytical models [e.g. Hertz, Derjaguin–Muller–Toporov (DMT)] used to interpret the data, all of which make the cross-study comparison of indentation moduli challenging. Further, it can be seen, in comparison with Table 2, that the indentation moduli seem to be generally considerably lower than Young's modulus found for subcellular patches of the cell wall in tensile testing. Differences also exist with Young's moduli obtained from tissue-scale tension tests. As will be discussed later, this might be related to the cellularity of the tissue structure.

Listening to the wall: acoustics-assisted measurements of cell mechanics

Acoustics are employed in various imaging and elastography techniques, such as in some types of AFM (for instance refer to Stan and Solares, 2014). Ultrasonic encoding of light in ultrasound-modulated optical or fluorescence imaging has been demonstrated to enable acquisition of deep-tissue images of biological materials (Wang *et al.*, 2012). However, acoustic waves can be used directly for imaging and mechanical testing of biological materials. Detection of the changes in frequency and amplitude of sound upon interacting with the sample, such as in scanning acoustic microscopy, or registering the energy shift of photons upon interacting with the acoustic phonons★—spontaneous or stimulated acoustic waves—in the sample structure can reveal information about the mechanical behavior of the sample.

Acoustic microscopy can be used for non-destructive imaging and mechanical characterization at the surface and subsurface of biological materials. Scanning acoustic microscopy is a widely used version of acoustic microscopy. In this technique, the piezoelectric transducer converts the electric signal to an acoustic wave focused into a beam by a lens. There are transmission and reflection modes of scanning depending on the type of waves collected by the receiver (Fig. 2). Passing through the coupling fluid, the acoustic beam enters the sample. The acoustic wave can be reflected, scattered, or attenuated. The portion of the acoustic wave reflected off the specimen is collected back at the transducer that is in listening mode and is then converted into an electric signal. Variations in amplitude and frequency between the probing and reflected signals are recorded. The coefficient of reflection of the sound wave at interfaces present in the specimen is correlated to their acoustic impedance★ mismatch. The acoustic impedance is correlated with the mass density and longitudinal modulus★ (in the direction of sound propagation) of the specimen. Therefore, the data acquired from the reflected sound can be used to reconstruct the stiffness map of the specimen (Rupin *et al.*, 2009). The resolution for scanning acoustic microscopy ranges from a few nanometers in superfluid helium to several micrometers (Foster and Rugar, 1983; Xi *et al.*, 2013), depending on several parameters including the acoustic beam spot size and the frequency. The resolution and depth of imaging have an inverse relationship. By increasing the frequency, higher resolution of imaging is possible (Rayleigh criterion) while the depth of imaging is forfeited. At a frequency of 2 GHz and room temperature, using deionized water, submicrometric resolutions have been achieved (Johnston *et al.*, 1979). For embryonic chicken heart muscle cells, at a sub-gigaHertz frequency and room temperature, subcellular compartments were resolvable with a resolution close to a micrometer (Weiss *et al.*, 2007), which reconfirms the potential of the technique to acquire a stiffness map of living cells at the microscale.

Application of scanning acoustic microscopy to study mammalian cell mechanics is relatively common. It has recently been suggested as a means for stain-free rapid diagnosis of cancer cells as their altered properties affect the speed and attenuation of sound waves when compared with healthy cells (Miura *et al.*, 2013). In plant biomechanics, acoustic elastography is perhaps the most underused technique. Tittmann and Xi (2014) used high-frequency scanning acoustic microscopy to investigate the feasibility of its application to study the mechanics of the primary plant cell wall. It was suggested that the measurements acquired with this technique are sensitive to changes in the onion epidermal cell walls upon application of pectinase. Modulation of pectin in the epidermis cell walls was indeed associated with a reduction in velocity of reflected waves, implying a reduced stiffness in the structure (Xi *et al.*, 2013; Tittmann and Xi, 2014). As can be observed from Tables 1 and 3, the value of Young's modulus found with this technique is over two orders of magnitude higher than the indentation modulus found with AFM indentation in the same study.

Application of scanning acoustic microscopy to study the mechanics of primary plant cell walls is not well explored, and the potential and limitations are largely unknown. In results

Table 2. *Young's (tensile) modulus for various plant species and cell types (updated versions of this table can be found at: www.plantbiomechanics.net/databases)*

Publication	TM (MPa)	Cell/tissue	Turgidity	Additional notes
Zamil *et al.* (2013)	3700±800 (L), 4900±1200 (T)	Subcellular patch, abaxial onion epidermis	Dehydrated	Cell wall thickness was used for calculations. The unusually high tensile modulus obtained here is likely to be due to dehydration of the cell wall segment.
Zamil *et al.* (2015)	374.6 (L)	Subcellular patch, abaxial onion epidermis	Hydrated	Cell wall thickness was used for calculations. First linear portion of stress–strain curve was chosen.
Zamil *et al.* (2017)	120.6±38.0 (L), 96.6±25.0 (T)	Tissue scale, abaxial onion epidermis	Hydrated	Force-controlled up to 0.25 N min⁻¹ loading rate. Cell wall thickness was used for calculations since the cells generally split open upon detachment of the abaxial onion epidermis.
Kim *et al.* (2015)	Dehydr.: 1900±300 (L), hydr.: 80±20 (L)	Tissue scale, abaxial onion epidermis	Hydrated and dehydrated	Cell wall thickness was used for calculations (abaxial epidermis splits open). Measured tensile modulus changed 20-fold upon dehydration.
Vanstreels *et al.* (2005)	17.5 (L) and 5 (T)	Tissue scale, adaxial onion epidermis	Turgid	Loading speed (µm s⁻¹): 1000, sample was rectangular, 10 mm in gauge length and 2 mm in width. Epidermis tissue layer thickness was used for calculations. Samples were immersed in water to eliminate or minimize contribution from turgor differential between samples.
Bidhendi et al. (unpublished results)	~6.5 (T)-15 (L)[†]	Tissue scale, adaxial onion epidermis	Turgid and plasmolyzed	Loading speed (µm s⁻¹): 20, sample was semi-dumbbell-shaped, 12 mm in gauge length, and 0.65 mm in width. Onion epidermis thickness was measured for several samples and averaged. Epidermis tissue layer thickness was used for calculations (~80 µm). Samples were immersed in water for turgid specimens and in mannitol solution for plasmolyzed group. Drops of the corresponding liquid were added on the samples during the experiment to keep them moist. The study suggested that the tensile behavior of isolated epidermis is non-linear and may be more accurately described using non-linear hyperelastic models. [†]Linear stiffness value measured for turgid epidermal tissue was: ~15.7 MPa (L) and ~8.6 MPa (T). These values were reduced upon plasmolysis to: 8.7 (L) and 6.6 (T).
Wei *et al.* (2001)	3.5–8[†]	Tissue scale, adaxial onion epidermis	Turgid and plasmolyzed[††]	Sample was rectangular, 18 mm in gauge length, and 3 mm in width. Epidermis tissue layer thickness was used for calculations (120 µm). Cyclic tensile testing was performed on samples. The first loading cycle was excluded from calculations since it differed considerably from the subsequent ones. [†]Modulus values were from averaging the results on L and T samples. The range corresponded to variation of different turgor pressure, with the tissue's tensile modulus increasing with turgor pressure. [††]Turgor pressure was varied by immersion in water or different mannitol concentrations; however, cells were never completely plasmolyzed.
Wei *et al.* (2006)	311±29 (L), 808±130 (T)	Subcellular scale-*Chara* internodal cell	Hydrated[†]	Sample was rectangular, varying in gauge length, and ~1.2 mm in width. Cell wall thickness (1.2 µm) was used for calculations. The significant size of *Chara* cells allowed for excision of subcellular patches from different angles with respect to the cells' longer growth axis. [†]During the experiment, the sample was immersed in water or an acid medium. Elastic modulus was shown to decrease with decreasing pH of the immersion solution.
Abasolo *et al.* (2009)	~20	Organ scale, hypocotyl/AT, dark-grown and 4–6 d old	Turgid[†]	Loading speed (µm s⁻¹): 10–15, sample was cylindrical, ~2.5 mm in gauge length. Diameters were measured under a microscope. Cross-section of sample was used for calculations. Cyclic tensile tests were performed. Data showed the slope of the first cycle to be less than the subsequent ones. For 6-day-old wild-type hypocotyls, this was a change from ~20 MPa in the first cycle to ~25 MPa in the third cycle. Xyloglucan mutants (*mur1*, *mur2*) and *qua2* with reduced HG pectin all showed significant decrease in tensile modulus compared with the wild type. [†]Water vapor was applied to prevent dehydration.

Table 2. *Continued*

Publication	TM (MPa)	Cell/tissue	Turgidity	Additional notes
Ryden *et al.* (2003)	~21–27	Organ scale, hypocotyl/AT, dark-grown and 4 d old	Turgid and plasmolyzed	Loading speed (µm s⁻¹): 30, sample was cylindrical, 3 mm in gauge length. Diameters of hypocotyls were measured and averaged. Cross-section of sample was used for calculations. Growing the samples in presence of 0.25 µM dichlorobenzonitrile, that inhibits cellulose synthesis, resulted in a 5-fold decrease in the tensile modulus and strength of hypocotyl, accompanied by a shorter but swollen organ phenotype. Various *mur* (xyloglucan) and *bot* (katanin) mutants also showed decreased tensile modulus and strength compared with the wild type, although affected to varying degrees. Removing the turgor was shown to increase the variance in test results. However, interestingly, the mean tensile modulus value was not significantly reduced upon plasmolysis (fig. 2 of the publication). Properties obtained in organ-scale tests are the average of behavior of different anatomical layers. In this case, an average between the primary cell walls and the secondary cell wall of the stele.
Saxe *et al.* (2016)	~10–47	Organ scale, hypocotyl/AT, dark-grown and 4–7 d old	Turgid	Loading speed (µm s⁻¹): 10, sample was cylindrical, 2 mm in gauge length. Effective cell wall cross-section was estimated from the sample density, and was used for stress calculations. Tensile modulus of 4-day-old samples was significantly lower than 5- to 7-day-old samples.
Cavalier *et al.* (2008)	~16	Organ scale, hypocotyl/AT, dark-grown and 4 d old	Turgid†	Loading speed (µm s⁻¹): 15, sample was cylindrical, 2.5 mm in gauge length. Cross-section of sample was used for calculations. Tensile test showed the xyloglucan mutants *xxt2* and *xxt1 xxt2* samples to have significantly reduced stiffness (~9 MPa) and tensile strength compared with the wild type. †Sample hydration was ensured by applying water vapor.

AT, *Arabidopsis thaliana*; L, longitudinal (along long axis of cell growth); T, transverse (perpendicular to long axis of cell growth); TM, tensile modulus.

published by Tittmann and Xi (2014), the contrast images seem to focus on the cell borders (i.e. anticlinal walls) and reveal less information on periclinal (outer) wall stiffness. This may be due to the fact that, since cells were not in their turgid state, periclinal walls were not bulgy and exposed. Interestingly, however, the technique has revealed details at the cell–cell interfaces potentially providing information on the middle lamella—the pectin-rich layer responsible for cell–cell adhesion in plant tissues. The typical output of scanning acoustic microscopy is acoustic impedance information that is not directly comparable with results of other types of measurements, often expressed as Young's modulus. Therefore, a challenge is to develop appropriate analytical and computational models to correlate the mechanical parameters. This is significant considering that the cell wall is anisotropic and its in-plane properties presumably differ significantly from those in its thickness (scanning direction). Moreover, the acoustic impedance map of the specimen is used to interpret its stiffness with the material density presumed to be known or constant over a region. This is not necessarily true because the cell wall thickness and density of the material in the porous★ wall network can vary. Therefore, use of complementary techniques to assess the spatial and temporal variation of the mass density such as microcomputed tomography is warranted to acquire elasticity information from the acoustic impedance data (Raum *et al.*, 2006; Rupin *et al.*, 2009). Another point is to ensure that ultrasonic waves do not change the cell wall properties thus potentially inducing artifacts. Pieczywek *et al.* (2017) showed that ultrasound treatment over several minutes could create voids in apple tissue. The authors suggest that the treatment increased the solubilization of pectin

in the cell wall, resulting in a dramatic decrease of the measured wall stiffness. While acquiring nanoscale maps of the cell wall stiffness is theoretically possible using scanning acoustic microscopy, so far the resolution for living cell applications has remained close to a micrometer. However, the resolution of this technique seems to be improving owing to the rapidly developing technology. Increasing the acoustic frequency *per se* to improve the resolution is not always practical. One reason is the strong attenuation of the sound waves in the coupling fluid. Attenuation increases with the frequency as the wave propagates. One way to avoid this is to decrease the traveling distance of the sound wave in the media which requires the generation of very short pulses of acoustic waves, so the desirable reflected wave is separable from the unwanted reflections. Combining picosecond ultrasonic with scanning acoustic microscopy, Che *et al.* (2015) used short-pulsed laser waves instead of piezoelectric transducers to generate ultrashort-pulsed acoustic waves and obtained a resolution of 100 nm using reflection mode scanning acoustic microscopy.

Colliding waves: Brillouin scattering elastography of the cell wall

Brillouin scattering microscopy is an optical elastography technique that takes advantage of scattering of light in interaction with acoustic waves to measure the mechanical properties of the light scattering material. Thermally induced acoustic waves occur naturally in all materials (Dil, 1982; Scarcelli and Yun, 2008; Ballmann *et al.*, 2017). The speed of acoustic waves in a
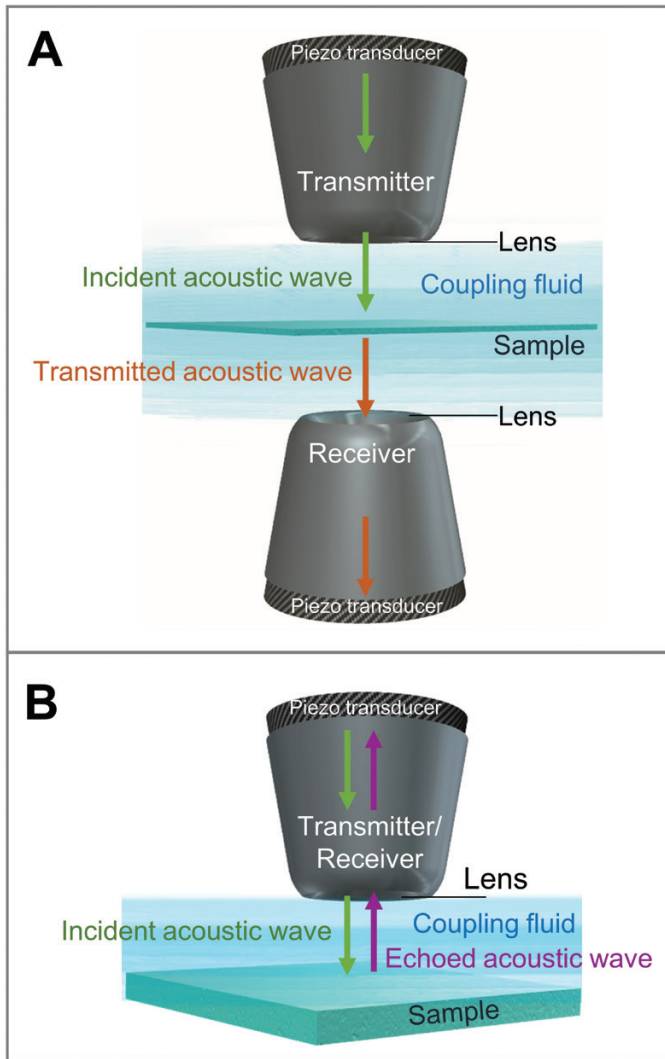
Fig. 2. Concept of scanning acoustic microscopy in (A) transmission and (B) reflection modes.

medium is affected by its atomic or molecular structure and hence its mechanical properties. Brillouin (1914) noted that the interaction of light and sound waves results in the scattering of light with a shift in its frequency (Brillouin frequency shift) and direction (Fig. 3). Light and sound alike possess both wave and particle properties. At the quantum scale, light consists of photon particles, and the quasi–particles of sound are termed phonons. The collision between these particles results in the exchange of energy between waves and changes their initial properties. The shift between the incident and scattered light is correlated with the speed and lifetime (related to damping properties of the medium) of phonons in the specimen and is used to determine the acoustic and consequently the viscoelastic properties of the material (Scarcelli and Yun, 2008). The application of Brillouin scattering for mechanical characterization of biological materials is not a very recent concept. For instance, Harley et al. (1977) used Brillouin scattering to study the mechanics of rat tail tendon. In recent years, the technique has gained considerable popularity in biomechanics as the technology evolved (for instance refer to the recent review by Scarcelli and Yun, 2008; Meng et al., 2016;

J. Zhang et al., 2016) and as the concept of Brillouin scattering is implemented in confocal systems (Scarcelli and Yun, 2008). 'Stimulated' Brillouin scattering microscopy is based on the same concept but benefits from a second laser beam (in addition to the one that is used to interact with the acoustic waves) used to induce short-pulsed acoustic vibrations in the sample to generate stimulated phonons in the specimen rather than relying only on naturally occurring phonons. This augments the efficiency of the Brillouin scattering, and higher spatial resolutions are attained (Mechri et al., 2009; Rakich et al., 2012; Dehoux et al., 2015). Since the current Brillouin scattering-based microscopes allow for non-invasive and label-free assessment of the 'hydromechanical' (Scarcelli et al., 2015) properties of the sample at high spatial resolution, a remarkable number of studies have been dedicated to assessing the capability of the method in biomechanical evaluation of biological tissues in the past few years. Brillouin scattering microscopy measurements of local stiffness moduli generally report a submicron resolution, similar to that of a conventional confocal microscope, with some variations of the technique reporting a resolution as good as 10 nm that has enabled imaging of the fibrillar structures of cells (Dehoux et al., 2015). Numerous reviews have been published over the past year covering different aspects of Brillouin and stimulated Brillouin microscopy, including the timeline of development and application, the theory, and the nature of the measured properties (Scarcelli et al., 2015; Wu et al., 2017, Preprint; Bottani and Fioretto, 2018; Garmire, 2018; Wu et al., 2018; Yun and Chernyak, 2018; Prevedel et al., 2019, Preprint).

Elsayad et al. (2016) combined fluorescence microscopy with Brillouin scattering (Fig. 3) to study the cell wall in onion epidermal cells and Arabidopsis hypocotyl and root cells. Cell wall stiffness and the influence of turgor pressure on the apparent stiffness of the cell wall were studied at submicrometer resolution. This study shows the potential of combining the two microscopy techniques to investigate the association of mechanical parameters, namely wall stiffness and turgor pressure, while monitoring wall chemistry and subcellular events using conventional fluorescence techniques. However, some conclusions in this study merit additional investigation, for instance the relationship between turgor pressure and the measured 'cytoplasmic stiffness'. As the authors mention, the term 'stiffness' in this context may be more related to the bulk modulus★ of the material rather than its Young's modulus (see Table 4 for compressibility★ as well as the difference between elastic moduli). Moreover, the images provided in these studies suggest that the technique detects a higher 'stiffness' for the nucleus than the periclinal cell wall. This seems inconsistent with results obtained with other methods that indicate that the stiffness of the nucleus is in the range of kPa (for example, see Guilak et al., 2000) while cell wall stiffness is typically in the MPa range as deduced using other techniques (Tables 1–3). Comparative and calibrating studies with other mechanical testing techniques may shed additional light on this matter. Gadalla et al. (2014) used stimulated Brillouin scattering microscopy to study the wall of onion cells with a submicron lateral and a nanometer in-depth resolution. The authors report a stiffness value of 13 GPa (see Table 3) for the cell wall in the

Table 3. *Elastic moduli of primary cell wall measured with other techniques (see also Tables 1 and 2 for comparison) (updated versions of this table can be found at: www.plantbiomechanics.net/databases)*

Publication	Measurement technique	Elastic modulus related to stiffness (MPa)	Cell/tissue	Turgidity	Additional notes
Sanati Nezhad et al. (2013b)	Bending of pollen tube, Lab-On-Chip	Young's modulus, 350 (L)	Pollen tube/Camellia	Turgid	Finite element modeling was used to uncouple the wall stiffness and turgor pressure. Several assumptions were made; a turgor pressure of 0.4 MPa was presumed in simulations. The result did not show to be sensitive to turgor pressure.
Tittmann and Xi (2014)	Acoustic microscopy	Young's modulus, 3300	Pavement cells of abaxial onion epidermis	Hydrated	The acoustic wave velocity demonstrated sensitivity to application of pectinase to epidermis samples, indicating potential for detection of changes in cell wall composition.
Elsayad et al. (2016)	Brillouin microscopy	Longitudinal elastic modulus, ~6000–12 000[†]	Epidermal cells/hypocotyl, AT	Turgid and plasmolyzed	Hypocotyl of double mutant *phyA phyB* showed decreased stiffness (longitudinal modulus) compared with the wild type (6500 MPa compared with 8500 MPa). [†]Values from fig. 5 of the publication.
Gadalla et al. (2014)	Brillouin microscopy	Longitudinal elastic modulus, ~13 000	Pavement cells of (probably adaxial) onion epidermis	Turgid	From the ratio of loss to storage longitudinal moduli obtained by this technique, it was suggested that the pectin matrix of the cell wall behaves similar to a glass-forming polymer networks in glassy state.

AT, *Arabidopsis thaliana*; L, longitudinal (along long axis of cell growth)
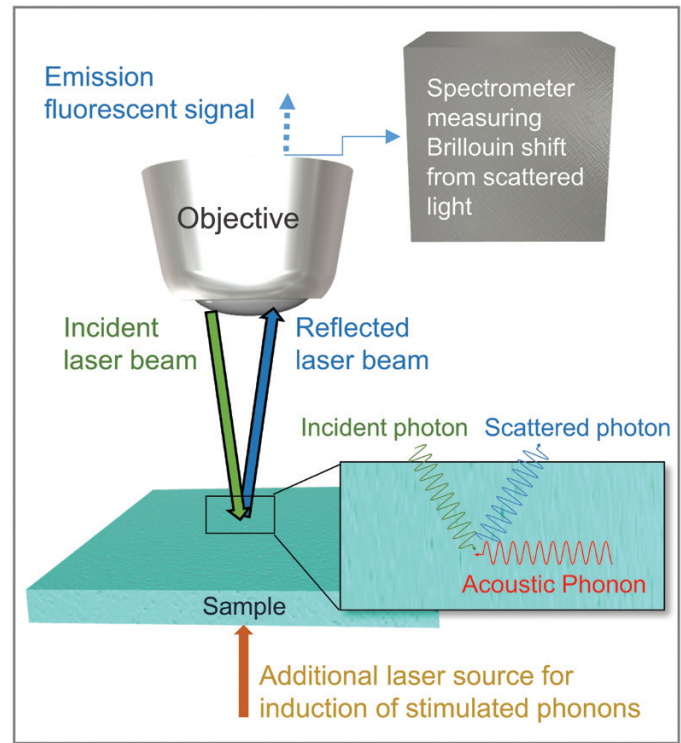

Fig. 3. Concept of Brillouin scattering microscopy for mapping of mechanical heterogeneity. The laser is focused on the sample. Interaction of the incident light wave and thermal acoustic waves results in scattering of light, changing its frequency and direction. The reflected light is collected back at the microscope and analyzed in the spectrometer to deduce the mechanical properties of the specimen (Scarcelli and Yun, 2008). This set-up allows simultaneous confocal fluorescent imaging of the specimen (e.g. Elsayad *et al.*, 2016). An additional beam can be used for induction of stimulated phonons in the specimen (e.g. Gadalla *et al.*, 2014).

onion epidermis. Based on the attenuation, they estimate the loss modulus, a measure of viscous effects, as 1.3 GPa. They suggest that the ratio of the loss to storage moduli (see complex modulus★) is close to values for glass-forming polymers at the glassy★ state. Therefore, the authors suggest that the rheology★ of the cell wall is governed by the glass-like behavior of the pectin–cellulose components. We wonder whether the glassy behavior of the cell wall is a result of the frequency at which the measurements occur and whether such a conclusion can be attributed to lower loading rates in other measurement techniques.

In studies performing Brillouin scattering mechanical characterization, information on the speed and lifetime of sound waves in the material is inferred from shifts in the scattered light measured by the spectrometer. These data are used to infer viscoelastic properties of the material. A main outcome of these studies is the longitudinal modulus (M) of the material (see Table 4). The longitudinal modulus is an elastic modulus, indicating the ratio of axial stress to strain, and provides a measure of the resistance of the material to axial deformation. As a result, this parameter has been used as a proxy for stiffness. However, the longitudinal modulus differs from Young's modulus since in the former the lateral strains are constrained. Therefore, the measured values have the potential to be reflective of material compressibility and water content

Table 4. *Glossary of key terms used in the text (tpdated versions of this table can be found under 'Plant cell mechanics glossary' at this site: www.plantbiomechanics.net/databases)*

Glossary

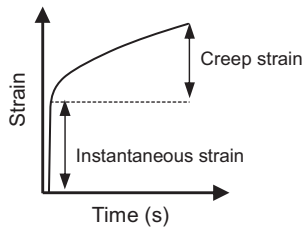| Term	Definition	Units—notes
Acoustic impedance	A measure of the resistance of the material to acoustic flow defined as the ratio of acoustic pressure to acoustic flow in a medium ($Z = \frac{P}{U}$).	Pa s m^{-3} Analogous to electrical impedance (resistance) where $Z\,(\text{ohm}) = \frac{V(V)}{I(A)}$, where V and I are voltage and electrical current, respectively.
Adhesion	Sticking and attraction of molecules or substances of different types.	See also cohesion*.
Anisotropy	Characteristic of a material whose properties differ depending on direction or orientation.	See also isotropy*.
Anticlinal wall	Cell wall perpendicular to the surface of the plant organ.	For epidermal cells, these walls constitute the side walls perpendicular to the plane of epidermis.
Boundary condition	Boundary demarcates the border of a physical object or a mathematical domain over which a system of differential equations is to be solved. Boundary conditions (BCs) set the constraints that are to be satisfied by the solution of differential equations at the border. In mechanics, boundary conditions can represent various parameters such as displacement, rotation, temperature, or fluid flow over different regions of border.	The deflection of a beam by a perpendicular force depends on how the ends of the beam are fixed (representing the BCs in this example). With a fixed BC, displacements and rotations are restricted. A pinned BC fixes the displacements but allows for rotations. A free BC allows all movements including vertical displacement.
Brittleness	Failure behavior of materials associated with abrupt fracture exhibiting little to no plastic deformation.	See also ductility*.
Bulk modulus	Ratio of volumetric stress to volumetric strain. An elastic modulus related to volumetric strain, providing a measure of resistance of the material to change of volume as a result of pressure applied in all directions ($K = -V\frac{\Delta P}{\Delta V}$). Note that the changes in pressure and volume are inversely related and the minus sign serves to produce positive K values. Bulk modulus is inversely related to compressibility*.	(N m^{-2} or Pa). The bulk modulus of water is close to 2.2 GPa. The relatively high bulk modulus of water has motivated various studies to assume that the bulk behavior of some of the soft biological tissues, with high water content, may be dominated by the bulk behavior of water rather than the elasticity of the solid phase resulting in an almost incompressible behavior. This, of course, depends on the structure of the tissue. Existence of pores allowing fluid flow under load changes this prospect.
Cell mechanics	Study of mechanical properties of the cell constituents, or study of forces applied to the cells or generated by the cells and applied to the cell's microenvironment and the resulting deformations.	Mechanotransduction, a branch of cell mechanics domain, is an umbrella term for various ways cells sense and respond to the mechanical forces.
Cohesion	Sticking of molecules or substances of the same type.	See also adhesion*.
Complex modulus	Also termed dynamic modulus. Ratio of stress to strain in dynamic analysis*. For instance, complex shear modulus is $G = G' + iG''$, where the real part (G′) is the storage shear modulus related to elastic properties of the material and the imaginary part (G″) is the loss shear modulus reflecting the viscous (dissipative) behavior of a material, respectively (i is the imaginary unit, $i^2 = -1$).	Also termed dynamics modulus. It is often plotted against a frequency spectrum and is an important measure in determining the frequency- and temperature-dependent behavior of materials.
Compliance	Inverse of stiffness*.	m N^{-1} or Pa^{-1}, depending on whether it is drawn from inverse of the slope of force–displacement or stress-strain data.
Compressibility	Reciprocal of bulk modulus. ($\beta = -\frac{1}{V}\frac{\Delta V}{\Delta P}$)	(m^2 N^{-1} or Pa^{-1}). See also bulk modulus* and elastic modulus*
Constitutive law	An equation describing the relationship between two physical quantities, for instance between the stresses applied to a material and the ensuing strains.	Can be termed differently, such as constitutive equation. Hooke's law* is an example of a constitutive law, that in its simplest form, describes the relationship between the force and elongation or compression of a spring.

Table 4. *Continued*

Glossary

Term	Definition	Units—notes
Creep	Gradual deformation of a viscoelastic material under constant stress over time. Creep deformation is partly recoverable and partly permanent upon removal of the load.	A purely elastic material deforms instantaneously in response to the applied stress.
Deformation (mechanics)	Refers to changes in shape of a body under application of loads (mechanical, thermal, etc.). Deformations can be reversible or irreversible. Deformation entails relative displacement of internal points of a body.	Pure displacement differs from deformation as in the former all points of a body move together and hold their relative position with respect to each other. This is also called rigid body displacement and is not associated with deformation or generation of internal stresses in the body. General displacement entails both rigid body displacement and deformation. See also strain*.
Ductility	Failure behavior of a material showing considerable plastic deformation prior to fracture or rupture.	See also brittleness*.
Dynamic analysis	Analysis of mechanical properties of the material by application of oscillatory (cyclic) stresses to the material and studying the resulting deformation of the material. Also referred to as dynamic mechanical analysis or DMA. See also complex modulus*.	Dynamic analysis is particularly useful for studying the viscoelastic properties of a material. It differs from static viscoelastic analysis as in creep or relaxation tests, since in DMA the load is time dependent. DMA is one of the major methods to assess important mechanical properties of the material such as viscoelasticity and glass transition temperature.
Elastic deformation	Deformation of a body that is fully recoverable upon removal of stress* with no residual deformation.	An ideally elastic material shows instantaneous deformation upon loading and instantaneous recovery upon unloading.
Elastic modulus	Any of the moduli defined for an elastic material, including Young's modulus*, bulk modulus*, shear modulus*, longitudinal modulus*, and Poisson's ratio*.	Note: an isotropic, linearly elastic material behavior can be defined with as few as two elastic moduli. Other elastic moduli can also be calculated if two independent constants are known. For instance, if Young's modulus (E) and Poisson's ratio (v) are known, shear modulus (G) and bulk modulus (K) can be calculated as: $G = \frac{E}{2(1+v)}$ and $K = \frac{E}{3(1-2v)}$ For anisotropic materials, more independent parameters are required to describe the deformation of the material. For a fully anisotropic material, this number is 21 constants. This can be further reduced by considering planes of symmetry. For an orthotropic material which has three planes of material symmetry, this number reduces to 9. For transversely isotropic materials that have an axis of material symmetry, that are of particular interest for modeling the plant cell wall if changes in thickness are ignored, five independent constants are needed. This number is considerably more manageable, but still challenging to measure or obtain. Note: sometimes elastic modulus is used to refer to Young's modulus of the material.
Extensibility (cell wall)	Potential of the cell wall material to deform irreversibly, resulting in expansive cell growth. Extensibility is related to the cell wall composition and mechanics, but also to other parameters such as temperature and enzymatic activity.	'Wall extensibility is like love. It conveys different meanings in different situations' (Cosgrove, 1993). Extensibility may be used to refer to various mechanochemical properties of the cell wall, such as creep behavior of wall or loosening, in the literature.
Failure (mechanics)	Loss of load-carrying capacity of the material under load application. Failure can be defined at various scales covering a range of microscopic to macroscopic phenomena.	
Flexural stiffness	Resistance of a body against bending deformation. For an elastic beam, for instance, it is related to Young's modulus (E) and the second moment of the area (I, defined based on the dimensions of cross-section), as well as the length and boundary conditions* of the beam.	Note: also referred to as bending stiffness or flexural rigidity. Flexural stiffness illustrates how, other than the material (incorporated as E), geometrical factors such as beam cross-section (input as I), influence the resistance of a structure against deformation.
Fracture strength	The stress at which the material fails by fracture.	(N m^{-2} or Pa)

Table 4. *Continued*

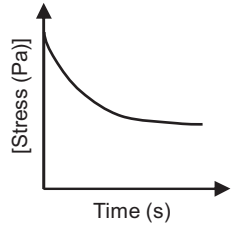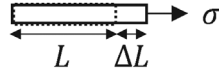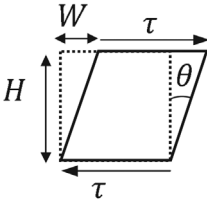| Glossary		
Term	**Definition**	**Units—notes**
Gauge length	The original distance between two ends of the sample in length considered as the original length of the sample in the calculation of strain in tensile test.	
Geometrical stiffness	Stiffness that, in addition to the stiffness of the constituent material, arises from the geometrical and structural features of the body, such as the second moment of the area. The resultant stiffness of the structure is due to both material and geometric aspects. See flexural stiffness*.	
Glassy state	State of disordered and amorphous structure of material in which atoms or molecules are in a 'frozen' state and cannot switch their neighbors or move around freely. The material in the glassy state is characterized by a stiff and brittle behavior.	This is in contrast to a 'rubbery' state in which the atoms and molecules in the material displace more freely and the material shows more flexibility and elasticity. Whether a material is in the glassy or rubbery state depends on its composition such as the molecular weight of its macromolecules, as well as the temperature and the frequency of measurements. The temperature around which the material transits from glassy to rubbery state is termed as the glass transition temperature, which is generally a spectrum rather than a value.
Homogeneity	Related to positional properties of the material. A material that is homogeneous with respect to a given parameter (e.g. stiffness*) has the same property (e.g. Young's modulus*) in all locations.	Is independent from isotropy*. A field/material can be isotropic but inhomogeneous, and vice versa.
Hooke's law	Law of elasticity, observed by Robert Hooke, stating that the deformation* of an object under application of force is proportional to the applied force. In basic form, this is expressed as $F=k\Delta l$, where F is force and Δl is change in length. k is the proportionality (spring) constant and is of ($N\ m^{-1}$) unit. k depends not only on the material the object is made of, but also on shape parameters such as its cross-sectional area.	Hooke's law is extended to the correlation between stress* and strain* in a continuous medium. For instance: $\sigma=E\varepsilon$. E is Young's modulus, ($N\ m^{-2}$ or Pa) and is an intrinsic property of the material. Note that Robert Hooke also discovered the building blocks of life for which he coined the term 'cells', by observing a sample of plant tissue.
Hysteresis (mechanics)	The phenomenon with a marked non-overlapping loading and unloading paths of material, indicating energy dissipation during deformation* (see Fig. 1A as a generic loading–unloading graph).	
Indentation modulus	A measure of resistance of body against indentation deformation*. It is often distinguished from Young's modulus due to several assumptions made in models used to obtain the indentation modulus.	Also referred to as apparent modulus or apparent (versus true) Young's modulus. Sometimes uncertainty in indenter tip geometry and tip–sample contact is also reflected in the term 'apparent' modulus. Note that apparent Young's modulus can be defined differently in various contexts and is not always related to indentation.
Isotropy	Material characteristic related to directional properties. An isotropic material has the same properties in all directions and is independent of homogeneity*. A field/material can be homogeneous but have directionally varying properties (anisotropy*).	In the case of the cell wall, anisotropy is typically only examined for the in-plane directions (rather than through the thickness) of the cell wall. Cell wall anisotropy is typically manifested by different mechanical properties (e.g. stiffness, extensibility, alignment of cellulose microfibrils) of the cell wall along and transverse to the cell's growth axis.
Linear elasticity	Elastic behavior of a material assuming it follows Hooke's law*, and a linear relationship between stress and strain. Most materials demonstrate linear elastic behavior at small strains. At larger strains, material and geometrical non-linearity can arise.	A special case of the more general non-linear elasticity theory.
Longitudinal modulus	Also known as constrained modulus, is an elastic modulus*, defined as the ratio of axial stress to axial strain. Unlike for Young's modulus* (E), for the longitudinal modulus (M) only axial strain* is allowed and lateral strains are zero.	Longitudinal modulus (M), speed of sound (V) and density (ρ) of material are correlated as: $V=\sqrt{\frac{M}{\rho}}$
Mechanical properties	Intrinsic (independent of quantity) physical properties of the material such as elastic modulus*, strength*, or anisotropy*. Mechanical properties of a material can be temperature and loading rate dependent, and determine how an object made from that material behaves under the application of internal or external loads.	
Mechanics	Branch of science that studies how forces (e.g. gravitation) act on bodies (fluids, solids; e.g. particles, red blood cells, wind, satellites, planets) and how bodies move, deform, and interact with one another as a result.	

Table 4. *Continued*

Glossary

Term	Definition	Units—notes
Periclinal wall	Cell wall parallel to the plane or surface of the plant organ.	For epidermal cells, these walls constitute the equivalent of the roof and the floor for the cells
Phonon	A quasiparticle for vibrational energy or disturbances in a material (e.g. sound), analogous to photon particles for electromagnetic radiation, e.g. light.	
Plasticity (mechanics)	Related to permanent or irreversible deformation* behavior of a material.	Plant cell expansion due to turgor is considered to be composed of elastic and plastic parts. The plastic part is termed as growth in some texts.
Poisson's ratio	Elastic modulus* defined as the ratio of lateral (perpendicular to stress application) to longitudinal (in direction of stress application) strains.	Dimensionless. For most isotropic materials, Poisson's ratio ranges between 0 and 0.5. Some rubbers have a Poisson's ratio close to 0.5, rendering them incompressible (see elastic modulus* for relationships). Cork has a Poisson's ratio close to zero. Negative Poisson's ratios are observed in auxetic materials, that due to their peculiar structure extend laterally when axially stretched.
Poroelasticity	Emerging elastic property of a fluid-filled porous solid resulting from a combination of viscoelasticity of the solid material and the effect of load-induced fluid flow through the porous network.	Retarded fluid flow in and between pores affected by pore structure and fluid viscosity* results in the emergence of time-dependent response of the fluid-filled solid medium similar to but distinct from viscoelastic behavior. See also viscoelasticity* and porosity*.
Porosity	Presence of voids within a material. Porosity allows for the interaction of two or more phases of solid, liquid, and gas. Porosity is often measured as volume fraction of voids with respect to the total volume of the material.	Voids can be interconnected, allowing fluid conduction in the solid medium, or can be isolated. The void fraction (porosity) and the characteristics (e.g. size and interconnectivity) of pores determine the permeability of the medium to fluid flow (hydraulic conductivity). See also poroelasticity*.
Relaxation	Gradual decrease of stress in a viscoelastic material under a constant strain.	See also creep*.
Rheology	Study of material flow or deformation under load, applicable to both fluids and solids.	
Stiffness (mechanics)	Measure of resistance of a material against deformation. A stiffer material deforms less than a softer material under the same load. The usage of stiffness varies in the literature and can, therefore, be ambiguous. While it sometimes refers to Young's modulus* of the material, it can also be used to refer to the spring constant (k=F/δ, or for rotational spring, k =T/θ, where F and T are force and torque, respectively. δ is displacement and θ is rotation).	(N m^{-1}, in the case of spring constant, N.m rad^{-1} in the case of rotational stiffness where rad stands for radian (unit for angle, SI), or Pa, in case it refers to the elastic modulus). Sometimes also referred to as rigidity. Definition of rigidity should not be confused with definition of a rigid body. A rigid body does not deform (see deformation* and strain*) under load. Semi-rigid bodies do. Note that stiffness does not always refer to an intrinsic property of the material. See also geometrical stiffness*.
Strain (mechanics)	A dimensionless value. Measure of relative changes (deformation) in dimensions of a body under load. It is calculated as the change, divided by the original value of the dimension. Corresponding to normal (σ) and shear (τ) stresses, are normal and shear strains.	Normal strain ($\varepsilon = \frac{\Delta L}{L}$) Shear strain ($\gamma = \frac{W}{H} = \tan\theta$) See also stress*.

Table 4. *Continued*

Glossary

Term	Definition	Units—notes
Strain rate	Rate of changes in strain* over time. Amount of strain applied per unit of time, descriptive of how quickly the material is loaded.	1/unit of time (s^{-1}, SI) Viscoelastic materials can demonstrate considerably different properties at different loading or strain rates.
Strain stiffening	Phenomenon associated with increasing stiffness* (elastic modulus*) of the material by strain*, resulting in a non-linear elastic response deviating from Hookean elasticity. Commonly observed in biopolymers due to mechanisms such as entanglement or straightening of polymer chains.	Also sometimes referred to as strain hardening. However, this usage is not preferred as in some contexts it can cause confusion. Strain hardening, or work hardening, is often reserved to refer to increased stress by strain in the plastic range of deformation in metals (strength) due to plastic flow, which occurs when metal atoms change neighbors under the load, irreversibly. Strain hardening corresponds to permanent deformations* and occurs due to mechanisms different from strain stiffening in polymer networks.
Stress (mechanics)	Force per unit area. There are various definitions of stress. Main types of stress are, however, normal (either tensile or compressive) and shear stresses. Normal stress (σ) is defined by the force acting perpendicular to the cross-section of the object, while shear stress (τ) acts parallel to the cross-section.	($N\,m^{-2}$ or Pa). See also strain*.
Stress softening	A phenomenon observed in cyclic tensile testing of many materials, marked by the reduction of stress* for a given strain* in successive cyclic load applications. In other words, to induce the same strain in the sample, lower stresses are required in reloading to a certain strain than the stress that was required in previous cycles (loading history dependence).	This phenomenon is also termed Mullins effect and arises due to damage in the material.
Tear/fracture resistance	Resistance of the material against propagation of tears or cracks in the material.	
Tensile modulus	For linear elasticity, alternative to Young's modulus*. Obtained under tension.	($N\,m^{-2}$ or Pa).
Torsion	A mode of deformation* entailing twisting of a body. Torsion gives rise to shear stresses* and strains*. See also strain*.	
Turgor pressure	Hydrostatic pressure built within plant and other walled cells due to fluid uptake by osmosis and presence of the cell wall. Turgidity is associated with the firmness of the plant structure and is thought to be required for wall expansion and cell growth.	($N\,m^{-2}$ or Pa). Turgor pressure in plant cells is generally suggested to be between a few tens of kPa to a few MPa.
Ultimate tensile strength	Maximum stress* a material can withstand under tension before fracture (see Fig. 4A).	($N\,m^{-2}$ or Pa).
Viscoelasticity	Behavior of a material exhibiting both elastic* (solid-like) and viscous* (fluid-like, dissipative) properties. The deformation* of a viscoelastic material under stress* depends on the rate of applied stress. At the molecular level, viscoelasticity arises due to slippage of bonds and friction between the macromolecules.	Viscoelastic deformation is not necessarily fully recoverable and plastic deformation may ensue. Anelasticity is a special case of viscoelastic behavior where the deformation is fully recoverable given enough time. See also creep* and relaxation*.
Viscosity	Measure of resistance of a fluid against deformation and flow, arising from internal friction between its layers.	There are several definitions of viscosity depending on the application. Pa s is the unit for dynamic viscosity which measures the internal resistance of the fluid to flow. Example: honey flows more slowly than water due to its higher viscosity.
Young's modulus	Ratio of stress* and strain* along one axis. The constant of correlation between stress and strain defined for linear elasticity* at small deformations where Hooke's law* applies.	($N\,m^{-2}$ or Pa). Often Young's modulus (E) is meant when the term elastic modulus* is used, or when stiffness* is referred to, although, in general, elastic modulus can refer to any of the other moduli defined for the elastic material. Note: the slope of the stress-strain curve is called Tangent modulus which becomes identical to Young's modulus at very small reversible strain range.

rather than the stiffness (Scarcelli and Yun, 2018; Wu *et al.*, 2018). This is significant since plant material consists mostly of water, which with a bulk modulus of close to 2.2 GPa is only minimally compressible. It has been discussed that changes in the longitudinal modulus are correlated with changes in Young's modulus of the sample, and studies have suggested

empirical relationships between the two parameters (Scarcelli *et al.*, 2011, 2015). However, some recent studies have expressed doubts on such a direct correlation and suggest that the measurements of the Brillouin microscopy may be more sensitive to the water content than the material's Young's modulus and that the correlation between longitudinal and Young's modulus vanishes when accounting for the water content (Wu *et al.*, 2017, Preprint; Scarcelli and Yun, 2018; Wu *et al.*, 2018). This is an issue that certainly warrants further investigation. As with acoustic microscopy, to calculate the longitudinal modulus, other quantities are needed such as the density of the material and its refractive index (for more details on the theory, refer to references presented thus far, e.g. Meng *et al.*, 2016). These data can be challenging to provide for heterogeneous structures

Fig. 4. (A) Generic engineering stress–strain graph for the loading portion of tensile testing. In the case of a linear elastic behavior, the slope of the elastic region is used to calculate Young's modulus of the material. In practice, the behavior of many biological materials is non-linear, even in the elastic (green) zone. Other parameters from the engineering stress–strain graph are: S_U, ultimate tensile stress (tensile strength); S_Y, yield stress; and S_F, fracture strength. Note that this graph depicts the generic behavior of a ductile material. In practice, the stress–strain curve of plant specimen may differ significantly. (B) Cutaway view of a thin membrane specimen fixed between two rings and stretched by hydraulic pressure in a bulge test.

such as the cell wall. As with the other techniques, the concern regarding loading rate and the frequency at which the measurements are performed applies. In this technique, the sound waves are studied at the high-frequency range of gigaHertz, adding another convoluting factor to the comparison of results with other techniques for the plant cell wall. Similar to acoustic microscopy, this optoacoustic technique seems also to report considerably higher measured stiffness compared with other techniques reviewed here (see Tables 1–3; Rupin *et al.*, 2009; Antonacci and Braakman, 2016), although, as discussed, a more in-depth comparison remains to be performed.

Brillouin scattering elastography and acoustic microscopy hold great potential for label-free non-invasive and *in vivo* measurements of plant cell viscoelastic properties. They allow obtaining data on cell wall mechanics on and below the cell's outer surface. The combination of acoustic techniques such as Brillouin scattering and Raman or fluorescence microscopy (see, for instance, Elsayad *et al.*, 2016) would open the door to the possibility of visualization and correlation of chemistry, mechanics, and development. Steps in this direction have been taken (Scarponi *et al.*, 2017) and we may soon be able to mechanically image the cell wall while following the dynamic changes in the cell wall components in real time. It will be essential to accompany these studies by validation that establishes to what extent the measurements obtained by this technique correlate with the cell wall mechanics related to morphogenesis.

The classic test: tensile measurement of cell wall properties

During tensile testing, the sample is stretched in either one (uniaxial) or two directions (biaxial), and the force required for the deformation is measured allowing for the determination of elastic, viscoelastic, and plastic properties. Uniaxial stretching is the most widely applied type of tensile testing in the characterization of biological materials (for instance, refer to Wei *et al.*, 2001, 2006; Ryden *et al.*, 2003; Peña *et al.*, 2004; Cavalier *et al.*, 2008; Abasolo *et al.*, 2009). The choice of uniaxial test for the cell wall is mainly justified by simpler device configuration, sample geometry, and straightforward calculations. We have recently reviewed the aspects to set up such a test (Bidhendi and Geitmann, 2018*b*). The application of tensile stress can be performed in a variety of ways. In general, loading is either carried out in a single application, increasing monotonically to rupture the sample or applied cyclically. Cyclic tensile tests can be performed by applying a smaller load that does not cause rupture and performing repeat loading–unloading. A generic stress–strain curve obtained from a uniaxial tensile test typically consists of three main regions (Fig. 4A, for monotonic loading), a 'toe' region potentially indicative of initial straightening of the specimen or rearrangement of its load-bearing fibers, an elastic regime that can be linear or non-linear, followed by the plastic deformation zone. The slope of the reversible (see elastic deformation) part of the graph is used to determine the elastic constants of the specimen (Young's modulus
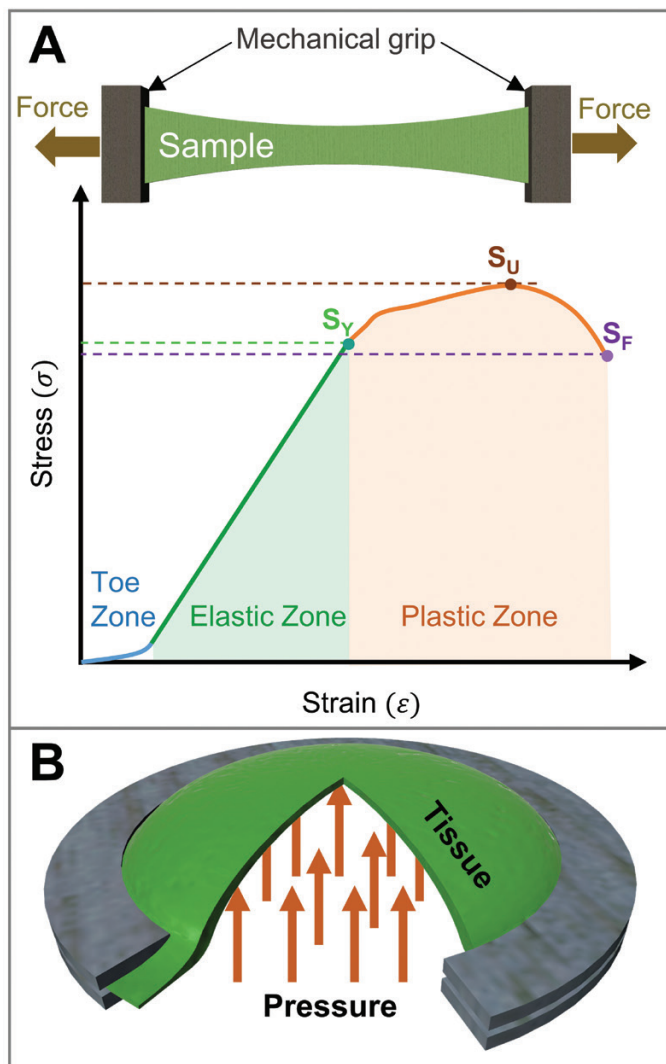
for a linearly elastic material). Ultimate tensile strength★ and fracture strength★ of the sample can also be calculated from the stress–strain graph of the monotonic tensile test. Tensile testing may be performed during loading or unloading, and the latter can be used to exclude the plastic deformation in the calculation of the elastic constants (Luczynski *et al.*, 2013; A.J. Bidhendi, H. Li, and A. Geitmann, unpublished results.). Cyclic tensile tests can be particularly insightful (Bidhendi and Geitmann, 2018*b*). Phenomena such as hysteresis★, stress softening★, and permanent deformations can shed light on the molecular composition of the plant cell wall including, but not limited to, how the amorphous and fibrillar phases of the cell wall composite material interact. For instance, it is often observed that the loading slope of the first cycle differs from the subsequent cycles (Spatz *et al.*, 1999; Köhler and Spatz, 2002; Vanstreels *et al.*, 2005; Wei and Lintilhac, 2007), a behavior that is also observed in animal tissues (Miller *et al.*, 2012). This has been attributed to straightening of wrinkles in the sample (Wei *et al.*, 2001), or changes occurring in the wall material (Vanstreels *et al.*, 2005) such as reorientation of cellulose microfibrils towards the direction of the applied stress (Kafle *et al.*, 2017). In some studies, to remove the considerable variability between cycles, the sample is 'preconditioned' by performing a number of loading–unloading cycles prior to actual tests. In many applications, especially in small deformations, the reversible deformation remains linear. However, material non-linearity may arise in tensile testing of biological samples due to their complex structure and under large strains. Therefore, appropriate material models must be used to describe the behavior of the samples when such effects are not negligible. Non-linear elastic models such as various hyperelastic functions can be fitted to the stress–strain curves to extract the elastic constants (for instance, Rashid *et al.*, 2012; A.J. Bidhendi, H. Li, and A. Geitmann, unpublished results). While the generic strain–stress curve presented here, typical of ductile★ metals, is useful to introduce a number of concepts, actual tensile graphs of biological tissues including plant specimens usually deviate from this behavior (for example, refer to Spatz *et al.*, 1999; A.J. Bidhendi, H. Li, and A. Geitmann, unpublished results).

Tensile testing of conventional materials at the macroscale is well defined by various standards such as American Society for Testing and Materials (ASTM) standards outlining the sample shape, dimensions, boundary★, and loading conditions. For instance, in many test standards, a dogbone shape is prescribed for flat specimens. This shape ensures a uniform strain, and that maximum stresses and fracture occur in the mid-region or gauge★ area of the specimen rather than near the clamp region. At non-uniform strains, the values found might deviate from the actual overall properties of the sample. Additionally, the standards allow for results of various studies to be comparable. However, tensile testing of biological materials, such as plant tissues, is inevitably associated with challenges, and the solutions are often custom and require outside the box approaches. Because of the delicate and miniature nature of certain plant samples, preparing predefined standard shapes is often challenging. Tensile tests of plant specimens have often been carried out on the tissue scale rather than on cell-sized

samples. A few exceptions are giant internode cells of algae (Métraux and Taiz, 1978; Toole *et al.*, 2001) or single fibers of the secondary wall (Sedighi-Gilani *et al.*, 2005; Burgert and Keplinger, 2013) where the single-celled or subcellular samples were large enough for conventional tensile testing configurations. In higher plants, the cells are much smaller, and extraction and handling of samples containing a few cells or a subcellular fragment is a formidable challenge. Even samples at tissue scale pose certain concerns to be accounted for. Tensile testing of specimens with dimensions below millimeter width requires manipulation and handling strategies suitable for their fragile nature (refer to an in-depth discussion of available techniques for manipulation, gripping, and force/strain measurement at increasingly smaller length scales in Gianola and Eberl (2009). Robinson *et al.* (2017) developed a miniature microscope-mountable tensile testing set-up that can perform tensile tests on plant tissues allowing visualization of individual cell deformation.

One challenge associated with sample handling is related to alignment with the force axis. Deviation from parallel alignment can cause a considerable error in measurements. This is especially critical in the case of plant tissues with pronounced anisotropy due to cellulose fiber orientation. Usually, establishing cellulose orientation and anisotropy cannot be done ad hoc but requires separate studies, and a misalignment resulting from the lack of information on this parameter can only further confound the results. Another critical factor is the aspect ratio of the samples. In plant research, sample dimensions are often limited by the dimensions of the organ under study (which is a considerable constraint with small model plants such as *A. thaliana*). Various studies have shown a significant dependence of the measured tensile modulus★ on the aspect ratio of the tensile specimen. Carew *et al.* (2003) conducted a comparative study on porcine tissue and found a considerable dependence of the measured stiffness on the sample aspect ratio. Interestingly, it was observed that the results can vary among specimens of different size even if the aspect ratio is kept constant. Similar size effect issues have been discussed in other studies pertaining to tensile properties of soft tissues (e.g. refer to Anssari-Benam *et al.*, 2012). The influence of sample size is not intuitive since, ignoring the inhomogeneity (see homogeneity★) of the tissue from which samples are taken, the material parameters are expected to be intrinsic to the material after the data are normalized by the length and cross-sectional area. Strain measurement inaccuracy is among the culprits for the discrepancy between values of the tensile modulus (Bidhendi and Geitmann, 2018*b*). For cellulose nanopaper specimens of different size and shapes, it was observed that the calculated tensile moduli converged to similar values when the strain was measured using a non-contact extensometer instead of using the displacement of the device cross-head which yielded large deviations between samples. The deviations had been generated by the compliance of the tensile testing device proper (Hervy *et al.*, 2017). In the same study, tensile strength remained size dependent and inversely related to sample size. This was conjectured to be due to the higher probability for a larger sample to include defects, such as voids, acting as weakest links determining the failure★ strength of the whole sample

(Hervy *et al.*, 2017). Another culprit has been the effect of the gripping end, or boundary condition⋆, in a more general sense, resulting in non-uniform strains in the sample. This issue has been shown to affect samples of different lengths differently, with samples shorter than an optimal threshold tending to generate sharp stress fields near the grips, resulting in an overestimation of the tensile modulus, and sample size dependence. Studies have been carried out to determine the optimal sample length to obtain consistent size-independent results (Sun *et al.*, 2005; Lievers *et al.*, 2010; Anssari-Benam *et al.*, 2012). Therefore, comparing the tensile properties of samples at different developmental stages must be approached with care as the results can be size dependent. Calibration and comparison studies to investigate this phenomenon in plant tissues and to establish standards for dimensions of plant specimens are deemed crucial.

Preparation of samples poses another significant challenge for tensile testing. Cutting of sample strips needs to be accurate, without tears and flaws at edges that would lead to stress concentration and premature failure. Rapid dehydration of specimens can alter the rheology of pectin and that of the cell wall (Bidhendi and Geitmann, 2016). Measurement of initial length and cross-section area, used in calculations, is also not without challenges. Saxe *et al.* (2016) studied the effect of age on the mechanics of the elongated zone (below the growth zone) in etiolated Arabidopsis hypocotyls. They correlated the mechanics of this zone to material density, geometry, and cellulose content. Their results seemed to suggest that the tensile stiffness of the samples increased from one developmental stage to the next. However, interestingly, a biochemical analysis showed a decrease in cellulose content of the cell walls over the same period. These confounding results may indicate that cell wall stiffness is not solely governed by its cellulose content but can also be modified by the reorientation of these fibers and other wall polymers such as pectin. On the other hand, this study also highlights the necessity to carefully account for all parameters such as the cross-sectional area of samples. It is tempting to use parameters measured directly from the experiment such as force and elongation. However, to exclude the effect of test- and sample-specific conditions such as cross-section in comparative studies, using derived parameters such as stress and strain is highly preferable albeit less convenient, as they allow determining intrinsic material properties. Judging from the published figures, the hypocotyls studied in Saxe *et al.* (2016) exhibited slightly higher cross-sections in the earlier developmental stage. This indicates one of the significant challenges faced in the tensile testing of plant tissues—the quantitative determination of initial parameters, and it highlights the necessity to establish best practice protocols enabling consistent measurements of sample dimensions (Burgert *et al.*, 2003; Sedighi-Gilani and Navi, 2007; Haag and Müssig, 2016).

Gripping of the specimens at the stretching ends is yet another critical technical consideration for tensile testing. Slippage and damage near the grips can affect the readings in seemingly successful experiments (Ng *et al.*, 2005; Sun *et al.*, 2005). Due to stress concentration and microscopic damage induced by the grip, many specimens break prematurely near the grip and sample interface. Such occurrences must be excluded

from the data pool. Glues, wires, and abrasive papers are among the methods used to attach samples to the load or displacement extensions to avoid or reduce slippage (Eder *et al.*, 2013). Glues such as cyanoacrylate or dental cement have been used, and epoxy has been suggested to alleviate the stress concentration in the attached end regions (Yu *et al.*, 2011; Eder *et al.*, 2013; Saxe *et al.*, 2016). However, application of glue can generate prestress in the specimen upon curing that needs to be released before the experiment. From our experience, the slippage at grips can emerge as a significant problem, particularly in experiments that take longer periods to complete, such as those performed at a lower strain rates⋆ or creep tests.

While measurements of elastic modulus or failure strength rely on the administration of a continuously increasing force till failure (tear or fracture), for evaluation of time-dependent properties a constant stress or strain is applied. These cases denote the creep or relaxation tests, respectively. A constant load is applied either by attaching a constant weight to one side of the sample or by establishing a force feedback loop that ensures a constant force as the sample is stretched between the load sensors. Creep tests are of particular interest in plant cell mechanics and morphogenesis contexts since they can elucidate the mechanisms of cell wall expansion under a constant force resembling that caused by turgor. Creep tests have contributed significantly to our understanding of the regulation of cell wall expansion by wall-modifying enzymes (Cosgrove, 1989; Keller and Cosgrove, 1995; Durachko and Cosgrove, 2009). The outcome of such experiments is often expressed as 'extensibility'⋆ (see Table 4) in cell wall-loosening studies, which may be defined as the dynamic creep of the cell wall as the wall material is being 'updated' by wall-modifying enzymes or other factors. The subtle difference that arises in some contexts between a traditional creep test and extensibility measurement is that the emphasis is on the ongoing nature of enzymatic modifications in the latter, while in former the properties of the inactive material are not modulated over time (for further discussion of this matter, refer to Cosgrove, 1993, 2016). In this context, it is worth noting the existence of two seemingly parallel views on cell growth. While in many studies, the mechanics of the cell wall, specifically its viscoelastic properties, have been explicitly or implicitly assumed to be relevant to cell growth, some researchers have expressed doubts on this issue. This alternative view does not dismiss the importance of cell wall mechanics but questions the extent to which the mechanical parameters of the cell wall material, such as Young's modulus, relate to cell growth. One of the main arguments is that growth is controlled by cell wall loosening, such as by the action of expansins, and this may not be sufficiently addressed by reporting alterations in elastic moduli of the wall. In short, the question of how stiffness correlates with cell wall loosening or extensibility is subject to ongoing debate. Terminology forms part of this debate, and the use of terms such as extensibility and compliance needs to be judicious (refer to Table 4 for definitions). We refer to Cosgrove (2016, 2018) for detailed discussion. Although a single parameter such as Young's modulus may, in some cases, not be sufficient to represent the changes associated with the growth of the cell wall due to enzymatic modification, any change in the cell wall can be described by a set of relevant

mechanical parameters. Therefore, the two views are not necessarily mutually exclusive, and studies are warranted to assess and link these two paradigms.

Uniaxial testing is the simplest tensile test condition but does not correlate well with the stress pattern the cell wall experiences *in vivo*. The stress exerted on plant cell walls by the turgor is biaxial, although the degree of stress anisotropy depends on the cell geometry. To simulate the *in vivo* loading conditions, multiaxial tension tests may, therefore, reveal novel aspects of wall behavior. Biaxial loading also eliminates the sample contraction during the test that can affect the alignment of cellulose microfibrils with regard to the sample axis. Contraction can irreversibly align microfibrils and produce strains that deviate from those occurring under biaxial stress *in vivo* (Chanliaud *et al.*, 2002). Biaxial stress can be applied by many methods, depending on factors such as specimen geometry (for example, refer to Chen and Matthews, 1993; Bursa and Zemanek, 2008; Olsson, 2011). A simple way of biaxial tension testing applicable to *in vivo* studies with intact cells is to record the changes in cell dimension with and without turgor pressure by osmotic treatment (Bidhendi and Geitmann, 2018*b*).

A more technically demanding type of biaxial tensile test apt for flat specimens is the hydraulic bulge test which entails application of a pressure gradient on the two faces of a thin film specimen held in a circular frame. This generates a spherical bulge (for instance, see Chen and Matthews, 1993; Bargel *et al.*, 2004) (Fig. 4B). The pressure and displacement of the emerging semi-spherical cap are used to plot the stress–strain graph. The system can also be used for creep or relaxation experiments, similar to the uniaxial tensile test. Several studies have attempted to formulate extraction of material parameters from stress–strain data obtained through this test. Computational modeling and simulation can also be used to inversely find the material parameters (Chanliaud *et al.*, 2002).

The classic implementation of tensile testing measures stress and strains, and produces a set of mechanical parameters for the overall sample ignoring its fine structure. Interpreting the mechanical properties of individual cell walls from the apparent tensile modulus determined through tissue scale tensile testing must, therefore, be approached with caution. A load applied to a strip of plant tissue is not necessarily carried equally by all cell walls which make up the tissue. Variations in cell size, geometry, and orientation can affect the load-carrying contribution of individual wall segments. Further, the intercellular interface material, the middle lamella, may also contribute to the tensile properties of the tissue (Zamil and Geitmann, 2017). Using videomicroscopy in conjunction with tensile testing can provide information on the strain field and non-uniform strain conditions such as through digital image correlation techniques (Hild and Roux, 2006; Pan *et al.*, 2009). Full-field measurements of the strain acquired by imaging (such as by monitoring the displacement of fluorescent fiducial markers) combined with an inverse finite element analysis (will be discussed later) have the potential to quantitatively determine the local material data (for an example of this approach in the plant context, refer to Kim *et al.*, 2015). Using this strategy allows determination of tissue level and subcellular stress and strains

from a heterogeneous strain field. This allows for closer scrutiny of properties of individual cell walls under tension. As with all other mechanical testing techniques, the effect of loading rate needs to be accounted for. This is due to the viscoelastic nature of biological samples. Depending on the speed, the measured behavior may reflect the properties of different populations of cell wall polymers. In general, at faster loading rates, the modulus value approaches 'unrelaxed' or 'instantaneous' values, and the material appears stiffer. At slower loading applications, the material appears softer and the modulus approaches a 'relaxed' value. It should be noted that the deformation behavior of a perfectly elastic material is independent of time. The rate dependency must be considered when comparing the results of different tensile tests, and the loading rate constitutes an important parameter to be reported along with other results. Tensile testing is a classic and powerful mechanical approach with direct relevance to the in-plane properties of cell walls. However, clearly, whether and to what extent the mechanical properties measured at multicellular scale can be attributed to the wall of individual cells warrants further studies. This is vital for correlating cell and tissue forces with growth (Kierzkowski and Routier-Kierzkowska, 2019). To ensure reproducible results, testing protocols are needed to assess the effect of and standardize variables such as the loading rate and other conditions described above.

Table 2 provides Young's modulus values from tensile test studies on various plant cells and tissues. It can be observed that the tensile moduli of plant cells and cellular patches vary several fold between outcomes of tensile tests and up to several orders of magnitude compared with the indentation moduli (Table 1). First, the dehydration of the tissue sample clearly has a dramatic effect on the tensile modulus. Unsurprisingly, but significantly, the hydration state of samples critically alters the compliance of primary plant cell walls (Table 2; Zamil *et al.*, 2013; Kim *et al.*, 2015). Secondly, there is a considerable variation between tensile moduli (Table 2) and the indentation modulus (Table 1) reported in various studies. Other than the above-mentioned challenges with respect to each test, a dominant factor differentiating their results is the mode of deformation they induce: tensile testing measures the in-plane tensile properties, compared with indentation that incorporates other aspects such as tissue deformation in its thickness (Milani *et al.*, 2011; Yakubov *et al.*, 2016). Since the primary cell wall is thought to be a construct made of individual layers that can, under specific circumstances, slip with respect to each other, deformation behavior of the cell wall in and out of plane can vary significantly. Thirdly, a considerable variation can be observed between tensile tests carried out at tissue and subcellular scales, with the latter yielding considerably higher values compared with the former. This effect, in part, can arise from the manner in which cross-sectional area and consequently stress are calculated (with stress equaling force divided by the cross-sectional area). Using the tissue thickness in the calculation of tensile modulus considers the cell lumen which, in practice, is not load bearing. This leads to lower calculated tensile moduli for the tissue compared with approaches that consider the effective cell wall thickness, as is the case when wall segments are tested. In addition to this, tissue as a cellular

structure can behave differently from its constituent material. Lastly, the method of calculating the modulus can affect the outcome. In most studies, a linear portion within the stress–strain curve is identified and its slope is reported as Young's modulus of the tissue. Bidhendi *et al.* (unpublished results) show for the onion epidermal tissue, that stress–strain behavior of primary plant tissue, at least when isolated from other tissue layers, may be best described using non-linear elastic functions. Basing the calculation on the concept of linear elasticity*, therefore, risks compromising reproducibility as the choice of the strain range over which the stress–strain curve appears to be linear is subjective. Reporting the range of stresses and strains used for calculations along with the calculated elastic modulus should therefore be best practice when basing calculations on linear elastic behavior. Despite all these, surprisingly, the tensile testing results on the plant cell wall could be categorized into three classes with somewhat clear upper and lower bounds (Table 2): (i) dehydrated plant samples are extremely stiff and their tensile modulus exceeds 1 GPa; (ii) scarce but valuable tensile tests on isolated cell wall segments that seem to report intermediate stiffness values close to 300 MPa (Wei *et al.*, 2006; Zamil *et al.*, 2015); and, finally, (iii) tissue and organ level tensile test data that report lower stiffness values compared with categories (i) and (ii), as they vary between a few to a hundred MPa, depending on several factors such as whether or not the tissue or the cell wall cross–section is used to calculate the stress. Values for onion epidermis or the Arabidopsis hypocotyl, for instance, converge reasonably well (for biological materials), despite the somewhat different testing conditions such as loading speed or sample geometry (Table 2). However, to draw firm conclusions, studies with larger data sets are required.

MEMS and microfluidics for high-throughput mechanical characterization of plant cells in mock *in vivo* conditions

Advances in micromachining techniques for integrated circuits have enabled fabrication of microelectromechanical systems (MEMS), miniature sized devices with components in the range of a few to hundreds of micrometers. MEMS can consist of passive mechanical microstructures such as cantilevers, or active components such as transducers and microelectronics integrated on or off chip. MEMS transducers can be classified as actuators or sensors. With these components, MEMS can sense and interact with their physical environment. To operate, MEMS transducers exploit various physical properties of materials such as electrostatic, magnetic, piezoelectric, or thermal effects. Force sensors can be as simple as a cantilever of known stiffness, deflection of which is used to calculate the force. The type of transducer is chosen based on considerations for the particular application such as the required maximum displacement, force, or resolution (Bell *et al.*, 2005). Tests carried out using MEMS typically fall in categories described in previous sections such as tensile testing or indentation (Bell *et al.*, 2005; Loh *et al.*, 2009), but they are executed on miniaturized testing
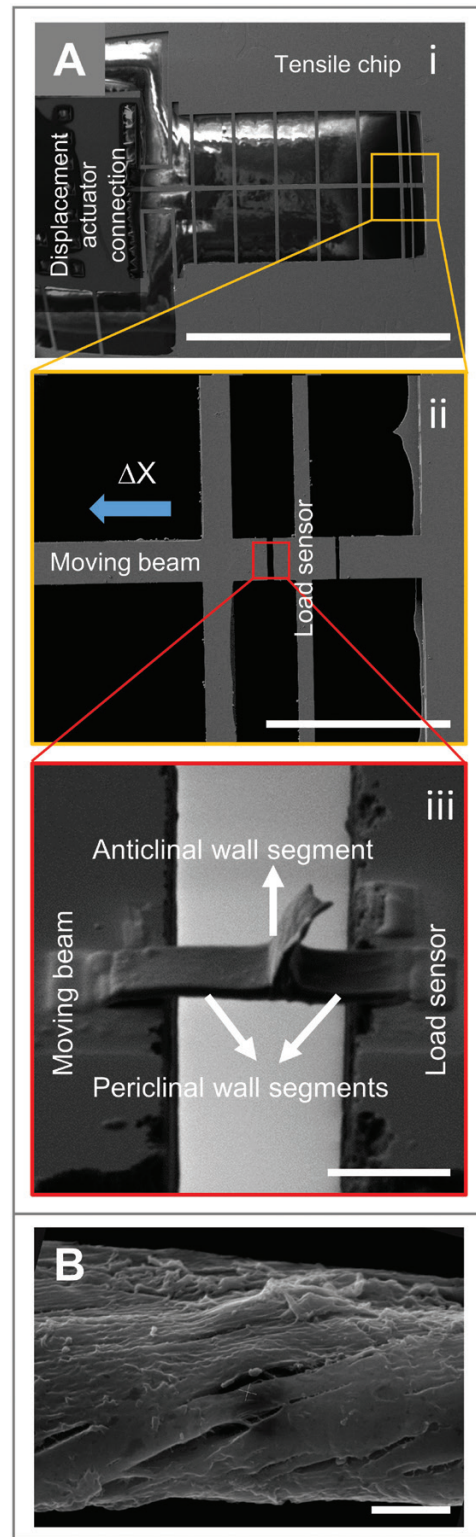

Fig. 5. (A) (i) and (ii) Scanning electron micrographs of the MEMS-based tensile device developed by Zamil *et al*. (2013). An off-chip displacement transducer moves the horizontal 'moving beam' that is stabilized by lateral beams. The force sensor is a beam of known compliance. Displacement of this beam is visually recorded. (iii) Fragment of an abaxial epidermal onion cell wall containing the periclinal walls and a portion of the anticlinal wall being stretched. (B) Cracks indicating the mechanical anisotropy in *Solanum* pollen tube wall following removal of pectin and chemical fixation. Reprinted from Aouar *et al*. (2010) with permission from Springer. Scale bars=4 mm [A (i)], 300 μm [A (ii)], 10 μm [A (iii)], and 3 μm (B).

frameworks that allow single-cell or subcellular manipulation and simultaneous visualization by light or electron microscopy.

One of the promising examples of a MEMS approach to quantify the mechanics of growing tissues is the work by Zhao *et al.* (2013) who developed a MEMS-based culture system to study the tensile properties of a microtissue construct of fibroblasts and type-I collagen. The system consisted of miniature PDMS (polydimethylsiloxane) wells each accommodating two vertical microcantilevers. The deflection of beams was induced by an external off-chip magnetic field and visualized using optical microscopy. Knowing the cantilever constants based on their material and geometry, the forces applied by the tip of the cantilevers to the specimen could be calculated. With this MEMS-based tensile device, the authors studied not only microtissue stiffness, but also active contractile forces generated by it.

In plant science, only very few MEMS-based studies have been published. Zamil *et al.* (2013) developed a novel method to perform microtensile tests on plant cell wall fragments—with dimensions of only a few micrometers—using an off-chip piezoelectric actuator with submicron force and displacement resolution (Fig. 5A). This approach allowed tensile testing of the cell wall specimen in different orientations with regard to the main axis of cell growth. Using focused ion beam milling, cell wall fragments as small as 5×15 μm were excised and mounted on the MEMS-based tensile device adapted from Haque and Saif (2002). The off-chip piezoelectric actuator delivered a controlled displacement to the MEMS chip. The MEMS chip composed of mechanically compliant structures was designed to transfer the displacement in a controlled on-axis manner to the cell wall specimen mounted on the chip. The forces delivered to the sample were calculable by observing the deflection of an on-chip beam, serving as force sensor, integrated perpendicular to the axis of loading, using SEM. Sample gripping was accomplished using focused platinum deposition. Using this tensile testing configuration, the authors characterized the tensile modulus and the fracture stress and strain of the microscale cell wall segment. The technique proposed by Zamil *et al.* (2013) has great potential for subcellular scale mechanical characterization of the cell wall, eliminating the complexity associated with the multicellularity of the tissue. However, it seems suitable only for dehydrated or rehydrated samples. Since SEM is required to monitor the deformations, the vacuum in the chamber has the potential to change the hydration state of the cell wall fragments, altering their mechanical behavior. This may explain the observed brittle★ fracture of the specimen. The results obtained with onion epidermis wall fragments indicated no significant difference in tensile modulus along the major and minor axes of cell growth, although the difference in fracture strengths was significant. Using MEMS at small scales, the physical behavior measured can deviate from macroscale experiments. At smaller scales, other forces such as capillary or surface adhesion can become prominent. Zamil *et al.* (2015) used static friction between the hydrated tissue and superpolished surface of the silicon chip to act as the grip, instead of glue. When operating at microscale dimensions, water loss can occur rapidly, resulting in a significant change in the mechanical properties. Continuous supply of water is

impossible when using surface adhesion forces as the gripping mechanism. Using this MEMS-based tensile technique, Zamil *et al.* studied the tensile properties of the middle lamella [Fig. 5A(iii)]. Interestingly, the authors found that the middle lamella, and the wall fragments containing middle lamella, are stronger than the wall fragments that lack this interface. Eventually, at microscale, the mechanical properties of the specimens such as Young's modulus can be sensitive to the size and the region of sampling, since the material in the small specimen can differ substantially from bulk properties of the tissue when tested with a larger scale tensile test. For instance, if a small region with a high concentration of aligned cellulose 'superbundles' is cut for microtensile testing, the results can differ significantly from an area with lower cellulose aggregation or lower anisotropy, while neither may reflect the overall tissue properties. The body of research in this field is small, and more studies are warranted to assess the potential of MEMS-based mechanical testing of plant cells.

Living cells are dynamic systems that sense and modify their mechanical environment and adapt to their surroundings because of such interactions. To study the relationship between the external cues and cell mechanics, devices are needed that can affordably simulate an adjustable physiological microenvironment and allow measurement of the mechanical properties of cells with minimal disturbances. Microfluidic devices enable the control and manipulation of minute volumes of fluids containing living cells. MEMS fabrication techniques can be used in the design of flow sensors, microchannels, microvalves, and micropumps to be used in microfluidic devices with biological applications (Ashraf *et al.*, 2011).

Fabrication of microfluidic devices from transparent materials such as PDMS provides optical properties required for live imaging of cellular events using conventional microscopes. Microfluidic devices have several advantages over conventional macroscopic cell visualization and assessment techniques including the possibility to mimic an *in vivo* microenvironment. This can be incorporated by fine-tuning the fluid flow, nutrients, chemical gradients, and placement of physical obstacles. Through smart design, live cells can be targeted at subcellular resolution by chemical agents such as hormones and growth factors, to study the physical response of cells (Sanati Nezhad *et al.*, 2014). By controlling fluid velocity to ensure a very low Reynolds number flow, forces applied to the cell can be finely adjusted (dominated by viscous forces proportional to the square of the fluid velocity). Results obtained using microfluidic devices have high reproducibility, and many cells can be tested in a short period. The high throughput and low cost of production of microfluidic devices enabling many parallel experiments give them an edge in studying the physical properties of cells.

For mammalian cells, application of microfluidics has been versatile such as in cell sorting and mechanical phenotyping in cancer diagnosis (Remmerbach *et al.*, 2009; Wang *et al.*, 2013; Dahl *et al.*, 2015). Agudelo *et al.* (2013) developed a microfluidic platform that allows manipulating single, tip-growing plant and fungal cells for mechanical testing—the TipChip. Sanati Nezhad *et al.* (2013b) used this platform to study the flexural stiffness★ of growing pollen tubes, the delivery organ of sperm

cells in plants. Growing pollen tubes were deflected by a laminar flow of a fluid oriented transversely to the pollen tube. A finite element method was used to model the pollen tube exposed to fluid drag, extracting Young's modulus of the cell wall. The calculations for this bending test showed little sensitivity to the absence or presence of a 0.4 MPa turgor pressure assumed in the inverse finite element modeling. In other studies, the TipChip was used to measure the penetrative forces of growing pollen tubes. In one approach, the elongating tubes' capacity to deform the elastic PDMS material forming narrow microchannels was used to calculate this parameter (Sanati Nezhad *et al.*, 2013a), whereas, in another, a calibrated cantilever made of PDMS was placed in the growth path of the tube (Ghanbari *et al.*, 2018). While the elastic PDMS walls of the microchannels and the cantilever represented a passive obstacle, Hu *et al.* (2016) used active deformation of the pollen tube by compression to calculate the turgor pressure and wall stiffness of lily pollen tubes. Inverse finite element modeling was used to provide a range of geometrical and mechanical parameters that could fit the compression experiment. The solutions of an undetermined system with more unknowns (i.e. wall's Young's modulus and thickness, and the turgor pressure) than the equations (modes of experiments) are not unique and were presented as a space of possible solutions. While the changes of turgor pressure due to large deformation during compression were not accounted for in the models, this approach is interesting and exemplifies the great potential of microfluidics for plant cell mechanics studies. The ease of the fabrication processes of microfluidic devices and the versatility of the experimental features can be exploited in many research approaches but have yet to be explored for multicellular plant tissues.

Learning from failure: tear and fracture as means to study plant cell mechanics and cell–cell adhesion

The mechanical testing techniques reviewed so far are minimally destructive to the cell or tissue. However, valuable insight on the structural properties of a material can also be obtained by observing its mechanical failure. Therefore, we propose that tear and fracture tests have the potential to yield information on mechanical properties of the plant cellular tissue including tear resistance★ and the geometry of fracture propagation. These have the potential to reveal data such as the orientation of cellulose microfibrils, as well as the type of polymers and degree of cross-linking between the constituents determining cell–cell adhesion, at both cellular and tissue scales. For instance, the orientation of fibers can affect the propagation of cracks in a composite material. In short-fiber-reinforced plastics, a crack applied at an angle to the principal fiber orientation changes direction to propagate along the fibers. When fibers are oriented at 0° or 90° to the loading direction, macroscopic observation suggests that the crack path is perpendicular to the loading direction (Tanaka *et al.*, 2014), but, microscopically, the crack follows a zig-zag path attempting to avoid crossing individual fibers. Consistent with this concept, Aouar *et al.* (2010) used the orientation of crack propagation in pollen tubes as

a proxy for cellulose orientation and overall mechanical anisotropy of the cell wall (Fig. 5B). The cracks were induced by partially removing pectin following chemical fixation. Actual tensile properties of the native wall might, therefore, be different depending on the relative contribution of pectin to the overall properties. Since cracks involve the entire thickness of the wall, this method may provide anisotropy information that is not attainable using methods such as SEM- or AFM-based cellulose visualization, which can only look at the innermost or outermost layers of the wall. Studying crack propagation in untreated, hydrated cell wall material will be crucial to investigate the role of pectin chemistry or parameters characterizing cellulose such as crystallinity or the anisotropy of the polymer network. Tearing also seems to be a promising approach to measure cell–cell adhesion (and wall material cohesion★), especially in different developmental stages of plant tissues and in mutants with cell adhesion defects (Verger *et al.*, 2018).

The dynamic duo: modeling and experiments for plant cell mechanics

Models attempting to examine the mechanics of cells fall into two categories: predictive (or forward) and interpretative (or backward) models. Predictive models can be surrogates used to test a concept and study an observed phenomenon by incorporating several rules and constraints, such as those used to simulate cell morphogenesis or the reversible movement of stomatal guard cells (Carter *et al.*, 2017; Bidhendi and Geitmann, 2018a; Lalitha Sridhar *et al.*, 2018; Weise and ten Tusscher, 2018, Preprint; Kennaway and Coen, 2019). Backward models are fit to experimental data to extract unknown parameters such as elastic moduli. Forward models can be physical or can encompass mathematical models of the plant cell. Application of physical models related to plant cell and tissue mechanics has remained scarce compared with mathematical models. One of the early examples of this class for plant cells is a physical model simulating the stomatal opening governed by turgor pressure using a pair of balloons locally reinforced by adhesive tapes, representative of radial reinforcement by cellulose (Aylor *et al.*, 1973). Braybrook and Peaucelle (2013) used a silicon replica of the Arabidopsis shoot apex to explore the effect of surface curvature on the registered force of indentation. Since a presumably isotropic material is used, changes in indentation force can indicate the influence of surface features on indentation readings. Durand-Smet *et al.* (2017) used a soccer ball to study the deformation behavior of a pressurized elastic shell, in order to shed light on dynamic loading deformation behavior of a single cell deformed between microplates, and to estimate the turgor pressure in isolated plant cells. Small dimensions encountered in plant tissues with primary cell walls often demand custom solutions to mechanical testing as outlined in previous sections. This ranges from the need for miniaturized testing devices, set-ups for *in situ* microscopy of strains, sample handling, employment of high-end sensors with a high signal to noise ratio, and maintaining proper temperature and humidity control during the test. Combined, these technical requirements result in a steep increase in cost as sample dimensions decrease. Development of additive manufacturing techniques has

opened the door to creating highly accurate 3D physical models (Stansbury and Idacavage, 2016; Zou *et al.*, 2016). Using 3D printing techniques, macroscopic models of cells and tissues can be produced for concept tests allowing for control over the level of details on and below the cell surface and scaling of the sample dimensions. 3D printing has already garnered great interest when used for designing cellular materials with emergent mechanical properties (Schaedler and Carter, 2016). This is due to the high spatial resolution in laying the solid and void phases and the possibility of using different types of printing materials. These, and especially the availability of anisotropic printing materials, make these techniques increasingly interesting for the fabrication and testing of plant cell and tissue analogs. Plants being cellular materials, we believe that the capabilities of this technology can open new doors to plant biomechanics research. For instance, tensile tests on 3D printed samples of plant tissues can provide insight on the behavior of the cellular tissue, including how tissue hierarchy, cell shape, and material anisotropy contribute to overall tissue mechanics. This allows for control over certain inputs, such as cell wall thickness and tissue homogeneity, that are hard to achieve with real plant specimens. 3D-printed cell and tissue analogs allow focusing on the variables of interest, eliminating other variables such as inherent variation between cells within a tissue or the effects of temperature or humidity. Scaling the sample dimensions also allows for testing on commonly available universal testing platforms instead of costly miniaturized machines with vibration isolation and sophisticated imaging set-ups. However, the use of 3D printing in the context of plant cell wall biomechanics is certainly not without its own pitfalls. For instance, the direction of printing (laying the material) and the layer thickness have been shown to affect the mechanical properties of the products (for example, see Farzadi *et al.*, 2014). The layered process has been shown to introduce a mechanical anisotropy in the product even with isotropic printing material. Nevertheless, additive manufacturing techniques such as 3D printing or subtractive manufacturing such as laser engraving can be complementary to *in silico* simulations in production and testing of plant cellular analogs at various scales. They can be used not only to validate simulations but to explore realms where the constitutive laws★ or numerical implementation are lacking or physical phenomena remain poorly understood, such as in exploring the mechanics of failure and fracture (for instance, see Mirkhalaf *et al.*, 2014). The power of these technologies for plant cell research is yet to be unleashed and requires dedicated studies. Note that here, by referring to 3D printing, we do not refer to 3D bioprinting (Vijayavenkataraman *et al.*, 2018), which constitutes a different class of additive manufacturing. 3D bioprinting is aimed at 3D construction of intricate biomimetic tissues using biological materials, such as living cells, as printing material. 3D bioprinting also has potential for plant cell growth research as it may allow for controlled construction of cell wall analogs using polysaccharides (Vancauwenberghe *et al.*, 2017).

Analytical or computational mechanical models have been widely used for both forward and backward models; for recent reviews of models of the primary plant cell wall, refer to Geitmann and Dyson (2014), Bidhendi and Geitmann (2018*a*), and Smithers *et al.* (2019). Analytical solutions are attractive due to their simplicity. However, often, owing to the complex behavior

of biological materials, sophisticated contact conditions between the experimental device (e.g. AFM probe tip) and the specimen and geometrical non-linearities, acquiring an analytical solution is not possible (Ali *et al.*, 2014). Even if analytical solutions exist, their range of application and reliability is limited by the assumptions made in their development. Interpreting material parameters from force–indentation data is often made based on the Hertz model which assumes the material as an infinite homogeneous half-space that is linearly elastic. It accounts only for small depths of indentation compared with the specimen thickness. To overcome these limitations, numerical models can be developed to incorporate more sophisticated material, geometry, and boundary conditions. The finite element modeling method has been used extensively and represents a promising solution for complex problems of material and geometrical non-linearity. Finite element-based modeling seems a promising tool to study the mechanics of morphogenesis in animal and plant tissues and cells (Hosseini *et al.*, 2014; Majda *et al.*, 2017; Hosseini and Taber, 2018). So far, several finite element models have been developed either to interpret (i.e. quantify) experimental data (Bolduc *et al.*, 2006; Dintwa *et al.*, 2011; Milani *et al.*, 2011; Hayot *et al.*, 2012; Routier-Kierzkowska *et al.*, 2012; Forouzesh *et al.*, 2013) or to analyze the behavior of plant cells (Cooke *et al.*, 1976; Hamant *et al.*, 2008; Dupuy *et al.*, 2010; Fayant *et al.*, 2010; Kha *et al.*, 2010; Kierzkowski *et al.*, 2012; Yi and Puri, 2012; Sampathkumar *et al.*, 2014; Bidhendi and Geitmann, 2018*a*, 2019; Bidhendi *et al.*, 2019).

To quantitatively analyze experimental data based on modeling, the choice of an appropriate material model is of vital importance. In most finite element studies of plant cell walls, the cell wall material behavior is considered as linearly elastic. However, this assumption only holds for small deformations, inconsistent with the fact that in many tensile experiments the strain may reach 50% or more (Pieczywek and Zdunek, 2014). Further, tensile testing of cell wall material has demonstrated non-linear behavior and strain stiffening★, which is typical of biological materials (Chanliaud *et al.*, 2002; Wang *et al.*, 2004; Erk *et al.*, 2010; Pieczywek and Zdunek, 2014; A.J. Bidhendi, H. Li, and A. Geitmann, unpublished results). In plant material, such strain stiffening may arise from either pectin (Michon *et al.*, 2004; Williams *et al.*, 2008) or cellulose–xyloglucan (Abasolo *et al.*, 2009) networks. Therefore, even in the elastic regime, a linear elastic modulus may not sufficiently describe the material behavior of the cell wall. Such elastic strain stiffening behavior may be inherent to the polymeric interaction of the cell wall and differs from the presumably plastic stiffening demonstrated in some of the so-called 'biphasic' behavior of the cell wall (Vanstreels *et al.*, 2005). The cell wall, similar to other biological materials, can exhibit strain-rate-dependent deformation behavior. The time or rate dependency can be attributed to either viscoelastic or poroelastic★ effects. In viscoelastic consideration, the time-dependent behavior of the cell wall can result from the viscous behavior of each class of wall biopolymers and their interactions such as those due to polymer chain slippage. Poroelastic material behavior results from fluid flow through the porous solid structure when hydrated. In addition, the solid structure (porous medium) itself can show viscoelastic behavior independent of the flow of the
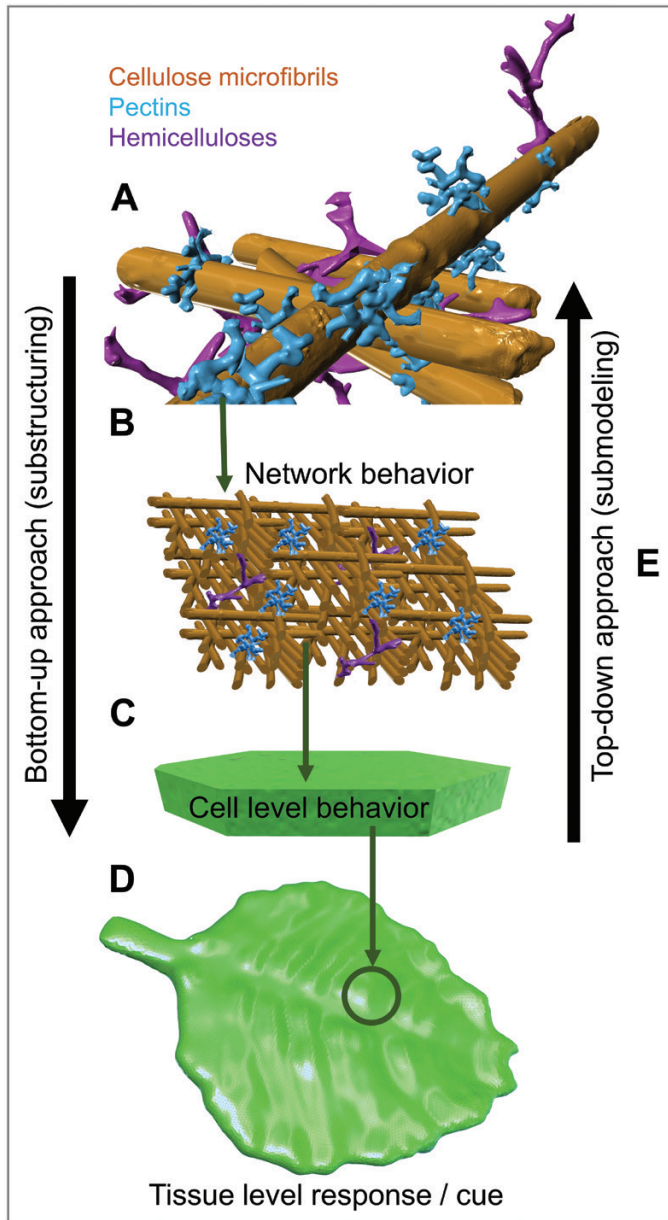
Fig. 6. Multiscale mechanical models are required to study the behavior, for example growth or response to environmental forces, of plant cells and tissues across scales. Depending on the scale investigated, a bottom-up or a top-down approach can be taken; (A–D) are steps in a bottom-up (substructuring) approach. (A) Properties of individual cellulose microfibrils, their bundles, pectin and hemicellulose molecules, and strength of chemical bonds between these components are assessed via *in vitro* assays and *in vivo* verifications. (B) Mechanical models can serve to investigate the cumulative behavior of the assembly of macromolecules, the individual components of which are from (A). Prominent examples of such studies are Kha *et al*. (2010) and Yi and Puri (2012). The results of this step should be compared against subcellular mechanical tests (e.g. Wei *et al.*, 2006; Zamil *et al.*, 2013). (C) Deformation or growth behavior of a cell or a representative volume consisting of cells is derived by incorporating the information from previous steps, at a subcellular scale. (D) Deformation and growth behavior of the tissue is reconstructed by superimposing the behavior of its building blocks from (C). The top-down process (submodeling) approach goes in the opposite direction. (E) Stresses and strains from a global model (e.g. tissue level) as a result of external loads or growth are known and are used as boundary conditions to predict and quantify the stresses and strains at smaller scales such as the cells at specific locations, stretch in cell membranes from global loads, or at the scale of cell wall components.

fluid phase. In both viscoelastic and poroelastic materials, at higher loading rates or short time scales, the polymer chains or the fluid have less chance to flow, and, as a result, the material exhibits a more solid–like or a stiffer behavior. Therefore, the time scale of the deformations, the state of hydration, and the composition of the specimen should dictate whether these considerations need to be incorporated into a model.

The shape and orientation of the cells *per se* may affect the apparent mechanical properties of the specimen (this differs from the effect of cell surface features on measured forces described in indentation testing). Multiscale modeling approaches can, therefore, be adopted to unravel the contribution of the cell wall from the effect of cellularity of the material. It should be noted that the cellularity effect arises due to existence of cell borders rendering the material discontinuous at microscale. This effect remains even if only the outermost layer of periclinal walls is used by stripping it off the tissue, as is the case when separating the abaxial onion epidermis. The partially remaining anticlinal walls continue to provide cellular geometry. Pieczywek and Zdunek (2014) investigated the behavior of onion epidermis tissue under tensile testing by finite element modeling considering realistic geometries of epidermal cells. In this study, the anticlinal walls were modeled based on the spatial pattern of cell borders extracted from micrographs, resulting in an open honeycomb-like structure neglecting the periclinal walls. The turgor pressure was represented with an elastic core for the cells. Such simplifications are generally performed due to significant computational load that more elaborate models would introduce. Further studies must assess the contribution of periclinal walls that presumably constitute the dominant portion of the load-bearing body in the epidermis, and that of the hydrostatic pressure on the mechanical behavior of plant tissues. Such an approach enables the study of cell shape in directional properties of the epidermis. Computation times for such a geometrically complex model can be minimized by reducing a structure consisting of repetitive units to a representative volume element (RVE) consisting of a small group of adjacent cells that can be assembled *in silico* to form extended tissues (Ptashnyk and Seguin, 2016; Zamil *et al.*, 2017) (Fig. 6C). Finally, aside from geometrical multiscale models of plant tissue and cells, understanding of cell wall behavior would be substantially enhanced if models could correlate the macroscopic deformation of plant materials to cell wall macromolecular structures such as cellulose orientation and alignment. A few studies have taken this path but are applied only to a spatially limited unit volume of the cell wall (Kha *et al.*, 2010; Yi and Puri, 2012; Nili *et al.*, 2015). For these models to be reliable, further information on mechanical properties of individual polysaccharides of the cell wall and their mechanical interactions are needed. Eventually, the availability of ever-improving computing power has provided us with the possibility of building massively multiscale models of the cell wall material and geometry to link the observed tissue level behavior to cell wall components—an insight we have so far sought indirectly. With such a philosophy in mind, two modeling strategies are particularly promising: substructuring (bottom–up) and submodeling (top-down). Substructuring can be broadly defined as the reconstruction and analysis of the behavior of a large–scale system

by integrating the behavior of its components (Fig. 6A–D). Conversely, in a submodeling approach, the large-scale behavior (global model) is presumed to be known, and one aims to zoom in to study the behavior of a component (submodel) resulting from the forces or deformations applied at the global scale. An example would be deducing the stretch induced in the plasma membrane at the subcellular level as a result of a wind-induced bending of the entire organ (Fig. 6). Although here illustrated on the same figure, these modeling approaches are carried out independently of each other.

Summary and outlook

Towards a unified understanding of the cell wall mechanics

Each technique used in the investigation of cell wall mechanics invariably comes with a set of strengths and limitations determining its relevance in different contexts. The quantitative data available for primary plant cell wall determined with various mechanical characterization techniques reveal significant variability and are indicative of substantial sensitivity to the test conditions but also the intrinsic differences in terms of the properties that are actually being measured (Tables 1–3). In this study, we listed some of the potential causes of these discrepancies. We hope that this will trigger benchmark studies performing further comparison of these techniques, especially the emerging ones, eventually leading to the determination of their suitability for the investigation of growing cell walls. While indentation or acoustic techniques can provide information on cell wall mechanics at the cell and subcellular scales, studies are required to address how these values are correlated with in-plane or otherwise growth-related mechanical properties of the cell wall. This is especially true for acoustics-related techniques that are less frequently used in the plant cell context, and studies must assess their usefulness in this regard. Data

---

Box 1.   Non-exhaustive list of points to consider when designing and interpreting an experiment that aims at determining plant biomechanical parameters

- What is the most pertinent testing method for the system intended to be investigated (e.g. is a subcellular resolution required)?
- How do the measured values relate to the growth-relevant properties of the wall?
  - How does indentation modulus relate to in-plane modulus of the cell wall? Does it predominantly measure the matrix (e.g. pectin) properties?
  - How does the tissue level information obtained from tensile testing relate to the cell wall properties at the cellular level?
  - How is cell wall anisotropy accounted for in any of the results?
  - How does cell wall stiffness (elastic moduli and/or viscoelastic properties) correlate with extensibility* (or growth)?
- Hydration
  - Is measurement of cell wall stiffness independent of the turgor pressure (e.g. verified by plasmolysis. See also Summary and outlook)?
  - Were sample properties changed by changes in the hydration state of wall polymers?
- Temperature
  - How sensitive are measurements to temperature fluctuations?
- How does experimental set-up affect the readings?
  - Are there standard experimental protocols (e.g. ASTM.) available? If not, can protocols/best practices be established?
  - How do the loading rate and stresses applied in the experiment correlate with cell growth-relevant forces and time scales?
  - What is the contribution of each cell wall polymer to the measured properties and how does this contribution change with loading frequency? In other words, what does each loading rate invoke?
  - Indentation: tip radius, tip shape, cantilever stiffness (if a cantilever-based system is used), device calibration (thermal vibrations, indenting a sample of known modulus, etc.), loading frequency, indentation model used to interpret the data (e.g. Hertz model, finite element models), sample global and local curvatures, data obtained from indentation or retraction, presence of cuticle, adhesion
  - Tensile testing: strain measurement method (e.g. extensometer, digital image correlation), device calibration and accounting for device compliance, gripping method and sample slippage, ensuring sensor linearity in the range of forces and temperatures used, the dependency of results on size and shape of samples, loading rate.
- Non-linearity:
  - Do testing conditions and material behavior allow the use of linear elasticity/small deformation assumptions?

acquired through indentation of the cell wall show considerable variation, even for the same type of cell and tissue (Table 1). Except for a few outliers, indentation moduli of the plant cell wall seem to be generally lower than the moduli measured in tension (Table 2). Tensile testing allows for direct measurement of the in-plane properties of the samples, with relatively straightforward calculations. However, this test is technically demanding due to challenges with gripping or sample damage which limit its usefulness for time-course studies of live samples. Further, inferring the subcellular data from tissue level tensile tests has yet to be established. The contribution of multiple anatomical layers, especially those with considerably different geometrical or material features such as the central stele of the hypocotyl, to the overall tensile behavior of the organ can create complex scenarios. Even for isolated tissues, such as onion epidermis, the shape and organization of the cells can make a significant contribution, in addition to the effect of the individual cell walls. Despite these, results from the tensile tests seem to be less scattered compared with the indentation test results (Table 2), if grouped according to their scale and sample hydration state. One reason for this may be the smaller number of parameters involved in setting up a tensile test compared with an indentation test. Another factor may be the tendency of the indentation tests with very fine probes to reflect 'very local' rather than bulk properties of the cell wall, resulting in great variations even between measurements performed on different locations of the same cell (Yakubov *et al.*, 2016). MEMS have shown great potential for the investigation of single cells and can incorporate all types of mechanical loads and real-time imaging on a chip at miniature scale. Yet, MEMS-based mechanical characterization of cells does not operate fundamentally differently from the aforementioned testing methods as they generally use one of the deformation modes described above, and are thus subject to the same considerations. Finally, fracture and tear of the plant cell wall and tissue may allow for the investigation of the cell wall molecular network, mechanical anisotropy, and cell adhesion, and future investigation of cell wall mechanics may benefit from the less explored realm of mechanical failure.

While one can argue whether a set of elastic moduli can adequately describe the growth of plant cells, as can be seen from the summary tables in this study, even these seemingly simple meters of cell mechanics show substantial divergence, even when acquired with the same measurement technique. While scattered findings acquired with different techniques can be attributed to the particular way each method deforms the cells and the cell walls, the differences for a given technique arise due to reasons such as loading rate, the extent of deformations, and how calculations are done (e.g. models used to interpret the data or measurement of initial values). In some publications, this information is not clearly reported, compounding reproducibility concerns (Nelson *et al.*, 2019). Regardless of this, due to variations between samples, and because of the different types of experimental set-ups, it is not surprising to see great variability between different studies, even those using the same type of technique. Further studies are needed to compare and benchmark the outcomes of different techniques and establish best practices. This will enhance our understanding of how

cell walls behave under different types of loading and permits the establishment of standard protocols to allow comparison of results between different laboratories. In Box 1, we have summarized a few points that we thought are helpful to consider prior to designing experiments and when interpreting results. Lastly, multiscale models can link the modification of the cell wall at the molecular level to cell and tissue behavior, which is important both for cell growth and for the cell's ability to sense and respond to the external mechanical cues. While parameters such as visco-elastoplastic properties of the cell wall can be studied experimentally, assessment of the stresses that arise in the cell wall during the plant cell growth is generally done indirectly—through modeling—as we still cannot visualize stresses in plant cells. In recent years, techniques such as insertion of microbubbles or introduction of fluorescently tagged reporter proteins have enabled visualization of mechanical forces between or within animal cells (Campàs *et al.*, 2014; Guo *et al.*, 2014). Development of similar sensor tools for plant cells to visualize the stress status in the cell wall or the magnitude of the turgor will be invaluable in studying the plant cell growth and morphogenesis.

Accounting for the contribution of turgor

In all types of measurements, turgor is a factor that can affect the perceived stiffness of the cell wall. It is known that plant cells and tissues are stiffer when turgid. To what degree the turgor pressure affects the measured stiffness-related properties of the cell wall, however, is not always obvious. For indentation tests, the available data (e.g. Table 1) suggest that the degree of contribution of turgor pressure to the measured stiffness largely depends on the size of the probing tip and depth of indentation. Very fine probe tips and limited indentation depths may reduce the contribution of the cell turgidity to the apparent stiffness. In tensile tests, plasmolyzed tissue generally appears softer, and the strain at rupture is increased. However, even in this test, the degree of contribution of the turgor pressure to the tensile modulus of the turgid tissue can vary. For instance, Bidhendi *et al.* (unpublished results) observed close to a 45% drop in the tensile modulus of the longitudinal adaxial onion epidermis upon plasmolysis, while this influence was seemingly only ~23% for the transverse specimens. Similarly, the reduction of tensile modulus upon plasmolysis of Arabidopsis hypocotyl was ~20% (Ryden *et al.*, 2003; see Table 2). The variation in contribution of the turgor pressure may be due to several factors including the initial water content of the tissue as well as the magnitude of strains. It can be postulated that the contribution of the turgor pressure may mask subtle variations in the cell wall mechanics and needs to be accounted for. In acoustics-related testing methods, the effect of the turgor pressure may be even more dramatic (Scarcelli and Yun, 2018; Wu *et al.*, 2018). A different concern arises from the potential direct effect on cell wall properties of osmotic treatments administered to maintain or eliminate turgor. This unexpected and interesting effect was suggested by Forouzesh *et al.* (2013) as their calculation of wall stiffness through indentation and inverse finite element analysis suggested that the cell walls of turgid samples immersed

in water were softer than the control (in air) and plasmolyzed samples. Aside from these considerations, the turgor pressure may not necessarily be identical for all cells in a given zone of the tissue. Combined, these issues highlight the importance of assessment of the turgor pressure and its contribution to the measured properties in studies of cell growth and measurements of cell viscoelastic properties.

Acknowledgements

References

Abasolo W, Eder M, Yamauchi K, et al. 2009. Pectin may hinder the unfolding of xyloglucan chains during cell deformation: implications of the mechanical performance of *Arabidopsis* hypocotyls with pectin alterations. Molecular Plant **2**, 990–999.

Agudelo CG, Sanati Nezhad A, Ghanbari M, Naghavi M, Packirisamy M, Geitmann A. 2013. TipChip: a modular, MEMS-based platform for experimentation and phenotyping of tip-growing cells. The Plant Journal **73**, 1057–1068.

Alcaraz J, Buscemi L, Grabulosa M, Trepat X, Fabry B, Farré R, Navajas D. 2003. Microrheology of human lung epithelial cells measured by atomic force microscopy. Biophysical Journal **84**, 2071–2079.

Ali O, Mirabet V, Godin C, Traas J. 2014. Physical models of plant development. Annual Review of Cell and Developmental Biology **30**, 59–78.

Amsbury S, Hunt L, Elhaddad N, Baillie A, Lundgren M, Verhertbruggen Y, Scheller HV, Knox JP, Fleming AJ, Gray JE. 2016. Stomatal function requires pectin de-methyl-esterification of the guard cell wall. Current Biology **26**, 2899–2906.

Anssari-Benam A, Legerlotz K, Bader DL, Screen HR. 2012. On the specimen length dependency of tensile mechanical properties in soft tissues: gripping effects and the characteristic decay length. Journal of Biomechanics **45**, 2481–2482.

Antonacci G, Braakman S. 2016. Biomechanics of subcellular structures by non-invasive Brillouin microscopy. Scientific Reports **6**, 37217.

Aouar L, Chebli Y, Geitmann A. 2010. Morphogenesis of complex plant cell shapes: the mechanical role of crystalline cellulose in growing pollen tubes. Sexual Plant Reproduction **23**, 15–27.

Ashraf MW, Tayyaba S, Afzulpurkar N. 2011. Micro electromechanical systems (MEMS) based microfluidic devices for biomedical applications. International Journal of Molecular Sciences **12**, 3648–3704.

Aylor DE, Parlange J-Y, Krikorian AD. 1973. Stomatal mechanics. American Journal of Botany **60**, 163–171.

Ballmann CW, Meng Z, Traverso AJ, Scully MO, Yakovlev VV. 2017. Impulsive Brillouin microscopy. Optica **4**, 124–128.

Bargel H, Spatz HC, Speck T, Neinhuis C. 2004. Two-dimensional tension tests in plant biomechanics—sweet cherry fruit skin as a model system. Plant Biology **6**, 432–439.

Baskin TI. 2005. Anisotropic expansion of the plant cell wall. Annual Review of Cell and Developmental Biology **21**, 203–222.

Beauzamy L, Derr J, Boudaoud A. 2015. Quantifying hydrostatic pressure in plant cells by using indentation with an atomic force microscope. Biophysical Journal **108**, 2448–2456.

Bell DJ, Lu TJ, Fleck NA, Spearing SM. 2005. MEMS actuators and sensors: observations on their performance and selection for purpose. Journal of Micromechanics and Microengineering **15**, S153.

Bidhendi AJ, Altartouri B, Gosselin F, Geitmann A. 2019. Mechanical stress initiates and sustains the morphogenesis of wavy leaf epidermal cells. BioRxiv doi: 10.1101/563403. [Preprint].

Bidhendi AJ, Geitmann A. 2016. Relating the mechanics of the primary plant cell wall to morphogenesis. Journal of Experimental Botany **67**, 449–461.

Bidhendi AJ, Geitmann A. 2018a. Finite element modeling of shape changes in plant cells. Plant Physiology **176**, 41–56.

Bidhendi AJ, Geitmann A. 2018b. Tensile testing of primary plant cells and tissues. In: Geitmann A, Gril J, eds. Plant biomechanics. Cham: Springer, 321–347.

Bidhendi AJ, Geitmann A. 2019. Geometrical details matter for mechanical modeling of cell morphogenesis. Developmental Cell doi:10.1016/j.devcel.2019.05.001.

Bidhendi AJ, Korhonen RK. 2012. A finite element study of micropipette aspiration of single cells: effect of compressibility. Computational and Mathematical Methods in Medicine **2012**, 192618.

Bolduc JE, Lewis LJ, Aubin CE, Geitmann A. 2006. Finite-element analysis of geometrical factors in micro-indentation of pollen tubes. Biomechanics and Modeling in Mechanobiology **5**, 227–236.

Bottani CE, Fioretto D. 2018. Brillouin scattering of phonons in complex materials. Advances in Physics: X **3**, 1467281.

Bou Daher F, Chen Y, Bozorg B, Clough J, Jönsson H, Braybrook SA. 2018. Anisotropic growth is achieved through the additive mechanical effect of material anisotropy and elastic asymmetry. eLlife **7**, e38161.

Boudaoud A. 2010. An introduction to the mechanics of morphogenesis for plant biologists. Trends in Plant Science **15**, 353–360.

Bozorg B, Krupinski P, Jönsson H. 2014. Stress and strain provide positional and directional cues in development. PLoS Computational Biology **10**, e1003410.

Braybrook SA. 2015. Measuring the elasticity of plant cells with atomic force microscopy. Methods in Cell Biology **125**, 237–254.

Braybrook SA, Peaucelle A. 2013. Mechano-chemical aspects of organ formation in *Arabidopsis thaliana*: the relationship between auxin and pectin. PLoS One **8**, e57813.

Brillouin L. 1914. Über die Fortpflanzung des Lichtes in dispergierenden Medien. Annalen der Physik **349**, 203–240.

Brulé V, Rafsanjani A, Pasini D, Western TL. 2016. Hierarchies of plant stiffness. Plant Science **250**, 79–96.

Burgert I, Frühmann K, Keckes J, Fratzl P, Stanzl-Tschegg SE. 2003. Microtensile testing of wood fibers combined with video extensometry for efficient strain detection. Holzforschung **57**, 661–664.

Burgert I, Keplinger T. 2013. Plant micro- and nanomechanics: experimental techniques for plant cell-wall analysis. Journal of Experimental Botany **64**, 4635–4649.

Burri JT, Vogler H, Munglani G, Läubli NF, Grossniklaus U, Nelson BJ. 2019. A microrobotic system for simultaneous measurement of turgor pressure and cell-wall elasticity of individual growing plant cells. IEEE Robotics and Automation Letters **4**, 641–646.

Bursa J, Zemanek M. 2008. Evaluation of biaxial tension tests of soft tissues. Studies in Health Technology and Informatics **133**, 45–55.

Butt H-J, Cappella B, Kappl M. 2005. Force measurements with the atomic force microscope: technique, interpretation and applications. Surface Science Reports **59**, 1–152.

Campàs O, Mammoto T, Hasso S, Sperling RA, O'Connell D, Bischof AG, Maas R, Weitz DA, Mahadevan L, Ingber DE. 2014. Quantifying cell-generated mechanical forces within living embryonic tissues. Nature Methods **11**, 183–189.

Carew EO, Patel J, Garg A, Houghtaling P, Blackstone E, Vesely I. 2003. Effect of specimen size and aspect ratio on the tensile properties of porcine aortic valve tissues. Annals of Biomedical Engineering **31**, 526–535.

Carter R, Woolfenden H, Baillie A, et al. 2017. Stomatal opening involves polar, not radial, stiffening of guard cells. Current Biology **27**, 2974–2983.

Cavalier DM, Lerouxel O, Neumetzler L, et al. 2008. Disrupting two *Arabidopsis thaliana* xylosyltransferase genes results in plants deficient in xyloglucan, a major primary cell wall component. The Plant Cell **20**, 1519–1537.

Chanliaud E, Burrows KM, Jeronimidis G, Gidley MJ. 2002. Mechanical properties of primary plant cell wall analogues. Planta **215**, 989–996.

Che S, Guduru PR, Nurmikko AV, Maris HJ. 2015. A scanning acoustic microscope based on picosecond ultrasonics. Ultrasonics **56**, 153–159.

Chen AS, Matthews FL. 1993. A review of multiaxial/biaxial loading tests for composite materials. Composites **24**, 395–406.

Cooke JR, De Baerdemaeker JG, Rand RH, Mang HA. 1976. A finite element shell analysis of guard cell deformations. Transactions of the ASAE **19**, 1107–1121.

Cosgrove DJ. 1989. Characterization of long-term extension of isolated cell walls from growing cucumber hypocotyls. Planta **177**, 121–130.

Cosgrove DJ. 1993. Wall extensibility: its nature, measurement and relationship to plant cell growth. New Phytologist **124**, 1–23.

Cosgrove DJ. 2005. Growth of the plant cell wall. Nature Reviews. Molecular Cell Biology **6**, 850–861.

Cosgrove DJ. 2016. Plant cell wall extensibility: connecting plant cell growth with cell wall structure, mechanics, and the action of wall-modifying enzymes. Journal of Experimental Botany **67**, 463–476.

Cosgrove DJ. 2018. Nanoscale structure, mechanics and growth of epidermal cell walls. Current Opinion in Plant Biology **46**, 77–86.

Cretin B, Sthal F. 1993. Scanning microdeformation microscopy. Applied Physics Letters **62**, 829–831.

Dahl JB, Lin JM, Muller SJ, Kumar S. 2015. Microfluidic strategies for understanding the mechanics of cells and cell-mimetic systems. Annual Review of Chemical and Biomolecular Engineering **6**, 293–317.

Dehoux T, Abi Ghanem M, Zouani OF, Rampnoux JM, Guillet Y, Dilhaire S, Durrieu MC, Audoin B. 2015. All-optical broadband ultrasonography of single cells. Scientific Reports **5**, 8650.

Dil J. 1982. Brillouin scattering in condensed matter. Reports on Progress in Physics **45**, 285.

Dintwa E, Jancsók P, Mebatsion H, Verlinden B, Verboven P, Wang C, Thomas C, Tijskens E, Ramon H, Nicolai B. 2011. A finite element model for mechanical deformation of single tomato suspension cells. Journal of Food Engineering **103**, 265–272.

Dupuy L, Mackenzie J, Haseloff J. 2010. Coordination of plant cell division and expansion in a simple morphogenetic system. Proceedings of the National Academy of Sciences, USA **107**, 2711–2716.

Durachko DM, Cosgrove DJ. 2009. Measuring plant cell wall extension (creep) induced by acidic pH and by alpha-expansin. Journal of Visual Experiments (25), e1263.

Durand-Smet P, Chastrette N, Guiroy A, et al. 2014. A comparative mechanical analysis of plant and animal cells reveals convergence across kingdoms. Biophysical Journal **107**, 2237–2244.

Durand-Smet P, Gauquelin E, Chastrette N, Boudaoud A, Asnacios A. 2017. Estimation of turgor pressure through comparison between single plant cell and pressurized shell mechanics. Physical Biology **14**, 055002.

Echevin E, Le Gloanec C, Skowrońska N, Routier-Kierzkowska A-L, Burian A, Kierzkowski D. 2019. Growth and biomechanics of shoot organs. Journal of Experimental Botany **70**, 3573–3585.

Eder M, Arnould O, Dunlop JW, Hornatowska J, Salmén L. 2013. Experimental micromechanical characterisation of wood cell walls. Wood Science and Technology **47**, 163–182.

Elsayad K, Werner S, Gallemí M, Kong J, Sánchez Guajardo ER, Zhang L, Jaillais Y, Greb T, Belkhadir Y. 2016. Mapping the subcellular mechanical properties of live cells in tissues with fluorescence emission-Brillouin imaging. Science Signaling **9**, rs5.

Erk KA, Henderson KJ, Shull KR. 2010. Strain stiffening in synthetic and biopolymer networks. Biomacromolecules **11**, 1358–1363.

Farzadi A, Solati-Hashjin M, Asadi-Eydivand M, Abu Osman NA. 2014. Effect of layer thickness and printing orientation on mechanical properties and dimensional accuracy of 3D printed porous samples for bone tissue engineering. PLoS One **9**, e108252.

Fayant P, Girlanda O, Chebli Y, Aubin CE, Villemure I, Geitmann A. 2010. Finite element model of polar growth in pollen tubes. The Plant Cell **22**, 2579–2593.

Fernandes AN, Chen X, Scotchford CA, Walker J, Wells DM, Roberts CJ, Everitt NM. 2012. Mechanical properties of epidermal cells of whole living roots of *Arabidopsis thaliana*: an atomic force microscopy study. Physical Review E **85**, 021916.

Forouzesh E, Goel A, Mackenzie SA, Turner JA. 2013. In vivo extraction of *Arabidopsis* cell turgor pressure using nanoindentation in conjunction with finite element modeling. The Plant Journal **73**, 509–520.

Foster J, Rugar D. 1983. High resolution acoustic microscopy in superfluid helium. Applied Physics Letters **42**, 869–871.

Fruleux A, Verger S, Boudaoud A. 2019. Feeling stressed or strained? a biophysical model for cell wall mechanosensing in plants. Frontiers in Plant Science **10**, 757.

Gadalla A, Dehoux T, Audoin B. 2014. Transverse mechanical properties of cell walls of single living plant cells probed by laser-generated acoustic waves. Planta **239**, 1129–1137.

Garmire E. 2018. Stimulated Brillouin review: invented 50 years ago and applied today. International Journal of Optics **2018**, 2459501.

Geitmann A. 2016. Actuators acting without actin. Cell **166**, 15–17.

Geitmann A, Dyson RJ. 2014. Modeling of the primary plant cell wall in the context of plant development. In: Assmann S, Liu B, eds. Cell biology. New York: Springer, 1–17.

Gershlak JR, Hernandez S, Fontana G, et al. 2017. Crossing kingdoms: using decellularized plants as perfusable tissue engineering scaffolds. Biomaterials **125**, 13–22.

Ghanbari M, Packirisamy M, Geitmann A. 2018. Measuring the growth force of invasive plant cells using Flexure integrated Lab-on-a-Chip (FiLoC). Technology **6**, 101–109.

Gianola D, Eberl C. 2009. Micro- and nanoscale tensile testing of materials. Journal of the Minerals, Metals and Materials Society **61**, 24–35.

Green PB. 1968. Growth physics in *Nitella*: a method for continuous in vivo analysis of extensibility based on a micro-manometer technique for turgor pressure. Plant Physiology **43**, 1169–1184.

Guilak F, Tedrow JR, Burgkart R. 2000. Viscoelastic properties of the cell nucleus. Biochemical and Biophysical Research Communications **269**, 781–786.

Guo J, Sachs F, Meng F. 2014. Fluorescence-based force/tension sensors: a novel tool to visualize mechanical forces in structural proteins in live cells. Antioxidants & Redox Signaling **20**, 986–999.

Guz N, Dokukin M, Kalaparthi V, Sokolov I. 2014. If cell mechanics can be described by elastic modulus: study of different models and probes used in indentation experiments. Biophysical Journal **107**, 564–575.

Haag K, Müssig J. 2016. Scatter in tensile properties of flax fibre bundles: influence of determination and calculation of the cross-sectional area. Journal of Materials Science **51**, 7907–7917.

Haase K, Pelling AE. 2015. Investigating cell mechanics with atomic force microscopy. Journal of the Royal Society, Interface **12**, 20140970.

Hamant O, Heisler MG, Jönsson H, et al. 2008. Developmental patterning by mechanical signals in *Arabidopsis*. Science **322**, 1650–1655.

Hamant O, Meyerowitz EM, Traas J. 2011. Is cell polarity under mechanical control in plants? Plant Signaling & Behavior **6**, 137–139.

Hamant O, Moulia B. 2016. How do plants read their own shapes? New Phytologist **212**, 333–337.

Han C-S, Sanei SH, Alisafaei F. 2016. On the origin of indentation size effects and depth dependent mechanical properties of elastic polymers. Journal of Polymer Engineering **36**, 103–111.

Haque M, Saif M. 2002. In-situ tensile testing of nano-scale specimens in SEM and TEM. Experimental Mechanics **42**, 123–128.

Harley R, James D, Miller A, White JW. 1977. Phonons and the elastic moduli of collagen and muscle. Nature **267**, 285–287.

Haupt A, Minc N. 2018. How cells sense their own shape—mechanisms to probe cell geometry and their implications in cellular organization and function. Journal of Cell Science **131**, jcs214015.

Hayot CM, Forouzesh E, Goel A, Avramova Z, Turner JA. 2012. Viscoelastic properties of cell walls of single living plant cells determined by dynamic nanoindentation. Journal of Experimental Botany **63**, 2525–2540.

Heinze K, Arnould O, Delenne JY, Lullien-Pellerin V, Ramonda M, George M. 2018. On the effect of local sample slope during modulus measurements by contact-resonance atomic force microscopy. Ultramicroscopy **194**, 78–88.

Heisler MG, Hamant O, Krupinski P, Uyttewaal M, Ohno C, Jönsson H, Traas J, Meyerowitz EM. 2010. Alignment between PIN1 polarity and microtubule orientation in the shoot apical meristem reveals a tight coupling between morphogenesis and auxin transport. PLoS Biology **8**, e1000516.

Hervy M, Santmarti A, Lahtinen P, Tammelin T, Lee K-Y. 2017. Sample geometry dependency on the measured tensile properties of cellulose nanopapers. Materials & Design **121**, 421–429.

Hild F, Roux S. 2006. Digital image correlation: from displacement measurement to identification of elastic properties—a review. Strain **42**, 69–80.

Hosseini HS, Beebe DC, Taber LA. 2014. Mechanical effects of the surface ectoderm on optic vesicle morphogenesis in the chick embryo. Journal of Biomechanics **47**, 3837–3846.

Hosseini HS, Taber LA. 2018. How mechanical forces shape the developing eye. Progress in Biophysics and Molecular Biology **137**, 25–36.

Hu C, Munglani G, Vogler H, Ndinyanka Fabrice T, Shamsudhin N, Wittel FK, Ringli C, Grossniklaus U, Herrmann HJ, Nelson BJ. 2016. Characterization of size-dependent mechanical properties of tip-growing cells using a lab-on-chip device. Lab on a Chip **17**, 82–90.

Hu S, Eberhard L, Chen J, Love JC, Butler JP, Fredberg JJ, Whitesides GM, Wang N. 2004. Mechanical anisotropy of adherent cells probed by a three-dimensional magnetic twisting device. American Journal of Physiology. Cell Physiology **287**, C1184–C1191.

Jäger A, Bader T, Hofstetter K, Eberhardsteiner J. 2011. The relation between indentation modulus, microfibril angle, and elastic properties of wood cell walls. Composites Part A: Applied Science and Manufacturing **42**, 677–685.

Johnston R, Atalar A, Heiserman J, Jipson V, Quate C. 1979. Acoustic microscopy: resolution of subcellular detail. Proceedings of the National Academy of Sciences, USA **76**, 3325–3329.

Kafle K, Park YB, Lee CM, Stapleton JJ, Kiemle SN, Cosgrove DJ, Kim SH. 2017. Effects of mechanical stretching on average orientation of cellulose and pectin in onion epidermis cell wall: a polarized FT-IR study. Cellulose **24**, 3145–3154.

Keller E, Cosgrove DJ. 1995. Expansins in growing tomato leaves. The Plant Journal **8**, 795–802.

Kennaway R, Coen E. 2019. Volumetric finite-element modelling of biological growth. Open Biology **9**, 190057.

Kha H, Tuble SC, Kalyanasundaram S, Williamson RE. 2010. WallGen, software to construct layered cellulose–hemicellulose networks and predict their small deformation mechanics. Plant Physiology **152**, 774–786.

Kierzkowski D, Nakayama N, Routier-Kierzkowska A-L, Weber A, Bayer E, Schorderet M, Reinhardt D, Kuhlemeier C, Smith RS. 2012. Elastic domains regulate growth and organogenesis in the plant shoot apical meristem. Science **335**, 1096–1099.

Kierzkowski D, Routier-Kierzkowska A-L. 2019. Cellular basis of growth in plants: geometry matters. Current Opinion in Plant Biology **47**, 56–63.

Kim K, Yi H, Zamil MS, Haque MA, Puri VM. 2015. Multiscale stress–strain characterization of onion outer epidermal tissue in wet and dry states. American Journal of Botany **102**, 12–20.

Kirmizis D, Logothetidis S. 2010. Atomic force microscopy probing in the measurement of cell mechanics. International Journal of Nanomedicine **5**, 137–145.

Köhler L, Spatz HC. 2002. Micromechanics of plant tissues beyond the linear-elastic range. Planta **215**, 33–40.

Kuznetsova TG, Starodubtseva MN, Yegorenkov NI, Chizhik SA, Zhdanov RI. 2007. Atomic force microscopy probing of cell elasticity. Micron **38**, 824–833.

Lalitha Sridhar S, Ortega JKE, Vernerey FJ. 2018. A statistical model of expansive growth in plant and fungal cells: the case of phycomyces. Biophysical Journal **115**, 2428–2442.

Landrein B, Hamant O. 2013. How mechanical stress controls microtubule behavior and morphogenesis in plants: history, experiments and revisited theories. The Plant Journal **75**, 324–338.

Levy R, Maaloum M. 2001. Measuring the spring constant of atomic force microscope cantilevers: thermal fluctuations and other methods. Nanotechnology **13**, 33–37.

Li QS, Lee GY, Ong CN, Lim CT. 2008. AFM indentation study of breast cancer cells. Biochemical and Biophysical Research Communications **374**, 609–613.

Lievers WB, Waldman SD, Pilkey AK. 2010. Minimizing specimen length in elastic testing of end-constrained cancellous bone. Journal of the Mechanical Behavior of Biomedical Materials **3**, 22–30.

Lim CT, Zhou EH, Quek ST. 2006. Mechanical models for living cells—a review. Journal of Biomechanics **39**, 195–216.

Lintilhac PM, Wei C, Tanguay JJ, Outwater JO. 2000. Ball tonometry: a rapid, nondestructive method for measuring cell turgor pressure in thin-walled plant cells. Journal of Plant Growth Regulation **19**, 90–97.

Loh O, Vaziri A, Espinosa H. 2009. The potential of MEMS for advancing experiments and modeling in cell mechanics. Experimental Mechanics **49**, 105–124.

Luczynski KW, Brynk T, Ostrowska B, Swieszkowski W, Reihsner R, Hellmich C. 2013. Consistent quasistatic and acoustic elasticity determination of poly-L-lactide-based rapid-prototyped tissue engineering scaffolds. Journal of Biomedical Materials Research. Part A **101**, 138–144.

Luo CJ, Wightman R, Meyerowitz E, Smoukov SK. 2015. A 3-dimensional fibre scaffold as an investigative tool for studying the morphogenesis of isolated plant cells. BMC Plant Biology **15**, 211.

Majda M, Grones P, Sintorn IM, et al. 2017. Mechanochemical polarization of contiguous cell walls shapes plant pavement cells. Developmental Cell **43**, 290–304.e4.

Malik I, Mirkhalaf M, Barthelat F. 2017. Bio-inspired 'jigsaw'-like interlocking sutures: modeling, optimization, 3D printing and testing. Journal of the Mechanics and Physics of Solids **102**, 224–238.

Marga F, Grandbois M, Cosgrove DJ, Baskin TI. 2005. Cell wall extension results in the coordinate separation of parallel microfibrils: evidence from scanning electron microscopy and atomic force microscopy. The Plant Journal **43**, 181–190.

Maver U, Velnar T, Gaberšček M, Planinšek O, Finšgar M. 2016. Recent progressive use of atomic force microscopy in biomedical applications. Trends in Analytical Chemistry **80**, 96–111.

Mazeran P-E, Odoni L, Loubet J-L. 2005. Curvature radius analysis for scanning probe microscopy. Surface Science **585**, 25–37.

Mechri C, Ruello P, Breteau J, Baklanov M, Verdonck P, Gusev V. 2009. Depth-profiling of elastic inhomogeneities in transparent nanoporous low-k materials by picosecond ultrasonic interferometry. Applied Physics Letters **95**, 091907.

Meng Z, Traverso AJ, Ballmann CW, Troyanova-Wood MA, Yakovlev VV. 2016. Seeing cells in a new light: a renaissance of Brillouin spectroscopy. Advances in Optics and Photonics **8**, 300–327.

Métraux JP, Taiz L. 1978. Transverse viscoelastic extension in nitella: I. Relationship to growth rate. Plant Physiology **61**, 135–138.

Michon C, Chapuis C, Langendorff V, Boulenguer P, Cuvelier G. 2004. Strain-hardening properties of physical weak gels of biopolymers. Food Hydrocolloids **18**, 999–1005.

Milani P, Braybrook SA, Boudaoud A. 2013. Shrinking the hammer: micromechanical approaches to morphogenesis. Journal of Experimental Botany **64**, 4651–4662.

Milani P, Gholamirad M, Traas J, Arnéodo A, Boudaoud A, Argoul F, Hamant O. 2011. In vivo analysis of local wall stiffness at the shoot apical meristem in *Arabidopsis* using atomic force microscopy. The Plant Journal **67**, 1116–1123.

Milani P, Mirabet V, Cellier C, Rozier F, Hamant O, Das P, Boudaoud A. 2014. Matching patterns of gene expression to mechanical stiffness at cell resolution through quantitative tandem epifluorescence and nanoindentation. Plant Physiology **165**, 1399–1408.

Miller KS, Edelstein L, Connizzo BK, Soslowsky LJ. 2012. Effect of preconditioning and stress relaxation on local collagen fiber re-alignment: inhomogeneous properties of rat supraspinatus tendon. Journal of Biomechanical Engineering **134**, 031007.

Mirkhalaf M, Dastjerdi AK, Barthelat F. 2014. Overcoming the brittleness of glass through bio-inspiration and micro-architecture. Nature Communications **5**, 3166.

Miura K, Nasu H, Yamamoto S. 2013. Scanning acoustic microscopy for characterization of neoplastic and inflammatory lesions of lymph nodes. Scientific Reports **3**, 1255.

Mosca G, Sapala A, Strauss S, Routier-Kierzkowska A-L, Smith RS. 2017. On the micro-indentation of plant cells in a tissue context. Physical Biology **14**, 015003.

Moulia B. 2013. Plant biomechanics and mechanobiology are convergent paths to flourishing interdisciplinary research. Journal of Experimental Botany **64**, 4617–4633.

Nakamura T, Gu Y. 2007. Identification of elastic–plastic anisotropic parameters using instrumented indentation and inverse analysis. Mechanics of Materials **39**, 340–356.

Nakayama N, Smith RS, Mandel T, Robinson S, Kimura S, Boudaoud A, Kuhlemeier C. 2012. Mechanical regulation of auxin-mediated growth. Current Biology **22**, 1468–1476.

Nelson N, Stubbs CJ, Larson R, Cook DD. 2019. Measurement accuracy and uncertainty in plant biomechanics. Journal of Experimental Botany **70**, 3649–3658.

Ng B, Chou S, Krishna V. 2005. The influence of gripping techniques on the tensile properties of tendons. Proceedings of the Institution of Mechanical Engineers, Part H: Journal of Engineering in Medicine **219**, 349–354.

Nili A, Yi H, Crespi VH, Puri VM. 2015. Examination of biological hotspot hypothesis of primary cell wall using a computational cell wall network model. Cellulose **22**, 1027–1038.

Olsson R. 2011. A survey of test methods for multiaxial and out-of-plane strength of composite laminates. Composites Science and Technology **71**, 773–783.

Ounkomol C, Xie H, Dayton PA, Heinrich V. 2009. Versatile horizontal force probe for mechanical tests on pipette-held cells, particles, and membrane capsules. Biophysical Journal **96**, 1218–1231.

Pan B, Qian K, Xie H, Asundi A. 2009. Two-dimensional digital image correlation for in-plane displacement and strain measurement: a review. Measurement Science and Technology **20**, 062001.

Parre E, Geitmann A. 2005. Pectin and the role of the physical properties of the cell wall in pollen tube growth of *Solanum chacoense*. Planta **220**, 582–592.

Peaucelle A, Braybrook SA, Le Guillou L, Bron E, Kuhlemeier C, Höfte H. 2011. Pectin-induced changes in cell wall mechanics underlie organ initiation in Arabidopsis. Current Biology **21**, 1720–1726.

Peaucelle A, Wightman R, Höfte H. 2015. The control of growth symmetry breaking in the Arabidopsis hypocotyl. Current Biology **25**, 1746–1752.

Peña MJ, Ryden P, Madson M, Smith AC, Carpita NC. 2004. The galactose residues of xyloglucan are essential to maintain mechanical strength of the primary cell walls in Arabidopsis during growth. Plant Physiology **134**, 443–451.

Perry SS. 2004. Scanning probe microscopy measurements of friction. MRS Bulletin **29**, 478–483.

Pieczywek PM, Kozioł A, Konopacka D, Cybulska J, Zdunek A. 2017. Changes in cell wall stiffness and microstructure in ultrasonically treated apple. Journal of Food Engineering **197**, 1–8.

Pieczywek PM, Zdunek A. 2014. Finite element modelling of the mechanical behaviour of onion epidermis with incorporation of nonlinear properties of cell walls and real tissue geometry. Journal of Food Engineering **123**, 50–59.

Prevedel R, Diz-Muñoz A, Ruocco G, Antonacci G. 2019. Brillouin microscopy—a revolutionary tool for mechanobiology? ArXiv 1901.02006. [Preprint].

Ptashnyk M, Seguin B. 2016. The impact of microfibril orientations on the biomechanics of plant cell walls and tissues. Bulletin of Mathematical Biology **78**, 2135–2164.

Radotić K, Roduit C, Simonović J, Hornitschek P, Fankhauser C, Mutavdžić D, Steinbach G, Dietler G, Kasas S. 2012. Atomic force microscopy stiffness tomography on living *Arabidopsis thaliana* cells reveals the mechanical properties of surface and deep cell-wall layers during growth. Biophysical Journal **103**, 386–394.

Rakich PT, Reinke C, Camacho R, Davids P, Wang Z. 2012. Giant enhancement of stimulated Brillouin scattering in the subwavelength limit. Physical Review X **2**, 011008.

Rashid B, Destrade M, Gilchrist MD. 2012. Inhomogeneous deformation of brain tissue during tension tests. Computational Materials Science **64**, 295–300.

Raum K, Leguerney I, Chandelier F, Talmant M, Saïed A, Peyrin F, Laugier P. 2006. Site-matched assessment of structural and tissue properties of cortical bone using scanning acoustic microscopy and synchrotron radiation muCT. Physics in Medicine and Biology **51**, 733–746.

Remmerbach TW, Wottawah F, Dietrich J, Lincoln B, Wittekind C, Guck J. 2009. Oral cancer diagnosis by mechanical phenotyping. Cancer Research **69**, 1728–1732.

Richmond PA, Métraux J-P, Taiz L. 1980. Cell expansion patterns and directionality of wall mechanical properties in nitella. Plant Physiology **65**, 211–217.

Robinson S, Huflejt M, Barbier de Reuille P, Braybrook SA, Schorderet M, Reinhardt D, Kuhlemeier C. 2017. An automated confocal micro-extensometer enables in vivo quantification of mechanical properties with cellular resolution. The Plant Cell **29**, 2959–2973.

Routier-Kierzkowska A-L, Smith RS. 2013. Measuring the mechanics of morphogenesis. Current Opinion in Plant Biology **16**, 25–32.

Routier-Kierzkowska A-L, Weber A, Kochova P, Felekis D, Nelson BJ, Kuhlemeier C, Smith RS. 2012. Cellular force microscopy for in vivo measurements of plant tissue mechanics. Plant Physiology **158**, 1514–1522.

Rupin F, Saïed A, Dalmas D, Peyrin F, Haupert S, Raum K, Barthel E, Boivin G, Laugier P. 2009. Assessment of microelastic properties of bone using scanning acoustic microscopy: a face-to-face comparison with nanoindentation. Japanese Journal of Applied Physics **48**, 07GK01.

Ryden P, Sugimoto-Shirasu K, Smith AC, Findlay K, Reiter WD, McCann MC. 2003. Tensile properties of *Arabidopsis* cell walls depend on both a xyloglucan cross-linked microfibrillar network and rhamnogalacturonan II–borate complexes. Plant Physiology **132**, 1033–1040.

Sampathkumar A, Krupinski P, Wightman R, Milani P, Berquand A, Boudaoud A, Hamant O, Jönsson H, Meyerowitz EM. 2014. Subcellular and supracellular mechanical stress prescribes cytoskeleton behavior in *Arabidopsis* cotyledon pavement cells. eLife **3**, e01967.

Sanati Nezhad A, Geitmann A. 2015. Tip growth in walled cells: cellular expansion and invasion mechanisms. In: Cuerrier C, Pelling A, eds. Cells, forces and the microenvironment. Boca Raton, FL: CRC Press, 335–356.

Sanati Nezhad A, Naghavi M, Packirisamy M, Bhat R, Geitmann A. 2013*a*. Quantification of cellular penetrative forces using lab-on-a-chip technology and finite element modeling. Proceedings of the National Academy of Sciences, USA **110**, 8093–8098.

Sanati Nezhad A, Naghavi M, Packirisamy M, Bhat R, Geitmann A. 2013*b*. Quantification of the Young's modulus of the primary plant cell wall using Bending-Lab-On-Chip (BLOC). Lab on a Chip **13**, 2599–2608.

Sanati Nezhad A, Packirisamy M, Geitmann A. 2014. Dynamic, high precision targeting of growth modulating agents is able to trigger pollen tube growth reorientation. The Plant Journal **80**, 185–195.

Sandhu AP, Randhawa GS, Dhugga KS. 2009. Plant cell wall matrix polysaccharide biosynthesis. Molecular Plant **2**, 840–850.

Sapala A, Runions A, Routier-Kierzkowska A-L, *et al*. 2018. Why plants make puzzle cells, and how their shape emerges. eLife **7**, e32794.

Saxe F, Weichold S, Reinecke A, Lisec J, Döring A, Neumetzler L, Burgert I, Eder M. 2016. Age effects on hypocotyl mechanics. PLoS One **11**, e0167808.

Scarcelli G, Kim P, Yun SH. 2011. In vivo measurement of age-related stiffening in the crystalline lens by Brillouin optical microscopy. Biophysical Journal **101**, 1539–1545.

Scarcelli G, Polacheck WJ, Nia HT, Patel K, Grodzinsky AJ, Kamm RD, Yun SH. 2015. Noncontact three-dimensional mapping of intracellular hydromechanical properties by Brillouin microscopy. Nature Methods **12**, 1132–1134.

Scarcelli G, Yun SH. 2008. Confocal Brillouin microscopy for three-dimensional mechanical imaging. Nature Photonics **2**, 39–43.

Scarcelli G, Yun SH. 2018. Reply to 'Water content, not stiffness, dominates Brillouin spectroscopy measurements in hydrated materials'. Nature Methods **15**, 562–563.

Scarponi F, Mattana S, Corezzi S, *et al*. 2017. High-performance versatile setup for simultaneous Brillouin-Raman micro-spectroscopy. Physical Review X **7**, 031015.

Schaedler TA, Carter WB. 2016. Architected cellular materials. Annual Review of Materials Research **46**, 187–210.

Sedighi-Gilani M, Navi P. 2007. Experimental observations and micromechanical modeling of successive-damaging phenomenon in wood cells' tensile behavior. Wood Science and Technology **41**, 69–85.

Sedighi-Gilani M, Sunderland H, Navi P. 2005. Microfibril angle non-uniformities within normal and compression wood tracheids. Wood Science and Technology **39**, 419–430.

Smithers ET, Lou J, Dyson RJ. 2019. Mathematical principles and models of plant growth mechanics: from cell wall dynamics to tissue morphogenesis. Journal of Experimental Botany **70**, 3587–3599.

Song Y, Bhushan B. 2006. Coupling of cantilever lateral bending and torsion in torsional resonance and lateral excitation modes of atomic force microscopy. Journal of Applied Physics **99**, 094911.

Spatz H, Köhler L, Niklas KJ. 1999. Mechanical behaviour of plant tissues: composite materials or structures? Journal of Experimental Biology **202**, 3269–3272.

Stan G, Solares SD. 2014. Frequency, amplitude, and phase measurements in contact resonance atomic force microscopies. Beilstein Journal of Nanotechnology **5**, 278–288.

Stansbury JW, Idacavage MJ. 2016. 3D printing with polymers: challenges among expanding options and opportunities. Dental Materials **32**, 54–64.

Sun W, Sacks MS, Scott MJ. 2005. Effects of boundary conditions on the estimation of the planar biaxial mechanical properties of soft tissues. Journal of Biomechanical Engineering **127**, 709–715.

Tanaka K, Kitano T, Egami N. 2014. Effect of fiber orientation on fatigue crack propagation in short-fiber reinforced plastics. Engineering Fracture Mechanics **123**, 44–58.

Tanguy M, Bourmaud A, Baley C. 2016. Plant cell walls to reinforce composite materials: relationship between nanoindentation and tensile modulus. Materials Letters **167**, 161–164.

Tittmann BR, Xi X. 2014. Imaging and quantitative data acquisition of biological cell walls with atomic force microscopy and scanning acoustic microscopy. In: Méndez-Vilas A, ed. Microscopy: advances in scientific research and education, Vol. **1**. Badajoz: Formatex, 161–172.

Toole GA, Gunning PA, Parker ML, Smith AC, Waldron KW. 2001. Fracture mechanics of the cell wall of *Chara corallina*. Planta **212**, 606–611.

Vancauwenberghe V, Mbong VBM, Vanstreels E, Verboven P, Lammertyn J, Nicolai B. 2017. 3D printing of plant tissue for innovative food manufacturing: encapsulation of alive plant cells into pectin based bio-ink. Journal of Food Engineering doi: 10.1016/j.jfoodeng.2017.12.003.

Vanstreels E, Alamar M, Verlinden B, Enninghorst A, Loodts J, Tijskens E, Ramon H, Nicolaï B. 2005. Micromechanical behaviour of onion epidermal tissue. Postharvest Biology and Technology **37**, 163–173.

Verger S, Long Y, Boudaoud A, Hamant O. 2018. A tension–adhesion feedback loop in plant epidermis. eLife **7**, e34460.

Vijayavenkataraman S, Yan WC, Lu WF, Wang CH, Fuh JYH. 2018. 3D bioprinting of tissues and organs for regenerative medicine. Advanced Drug Delivery Reviews **132**, 296–332.

Vlassak J, Ciavarella M, Barber J, Wang X. 2003. The indentation modulus of elastically anisotropic materials for indenters of arbitrary shape. Journal of the Mechanics and Physics of Solids **51**, 1701–1721.

Vlassak JJ, Nix W. 1994. Measuring the elastic properties of anisotropic materials by means of indentation experiments. Journal of the Mechanics and Physics of Solids **42**, 1223–1245.

Vogler H, Draeger C, Weber A, *et al*. 2013. The pollen tube: a soft shell with a hard core. The Plant Journal **73**, 617–627.

Wang CX, Wang L, Thomas CR. 2004. Modelling the mechanical properties of single suspension-cultured tomato cells. Annals of Botany **93**, 443–453.

Wang G, Mao W, Byler R, Patel K, Henegar C, Alexeev A, Sulchek T. 2013. Stiffness dependent separation of cells in a microfluidic device. PLoS One **8**, e75901.

Wang L, Hukin D, Pritchard J, Thomas C. 2006. Comparison of plant cell turgor pressure measurement by pressure probe and micromanipulation. Biotechnology Letters **28**, 1147–1150.

Wang YM, Judkewitz B, Dimarzio CA, Yang C. 2012. Deep-tissue focal fluorescence imaging with digitally time-reversed ultrasound-encoded light. Nature Communications **3**, 928.

Weber A, Braybrook S, Huflejt M, Mosca G, Routier-Kierzkowska A-L, Smith RS. 2015. Measuring the mechanical properties of plant cells by combining micro-indentation with osmotic treatments. Journal of Experimental Botany **66**, 3229–3241.

Wei C, Lintilhac PM. 2007. Loss of stability: a new look at the physics of cell wall behavior during plant cell growth. Plant Physiology **145**, 763–772.

Wei C, Lintilhac LS, Lintilhac PM. 2006. Loss of stability, pH, and the anisotropic extensibility of Chara cell walls. Planta **223**, 1058–1067.

Wei C, Lintilhac PM, Tanguay JJ. 2001. An insight into cell elasticity and load-bearing ability. Measurement and theory. Plant Physiology **126**, 1129–1138.

Weise LD, ten Tusscher KH. 2018. Discrete mechanical growth model for plant tissue. BioRxiv doi: 10.1101/459412. [Preprint].

Weiss EC, Lemor RM, Pilarczyk G, Anastasiadis P, Zinin PV. 2007. Imaging of focal contacts of chicken heart muscle cells by high-frequency acoustic microscopy. Ultrasound in Medicine & Biology **33**, 1320–1326.

Williams M, Vincent R, Pinder D, Hemar Y. 2008. Microrheological studies offer insights into polysaccharide gels. Journal of Non-Newtonian Fluid Mechanics **149**, 63–70.

Wu P-J, Kabakova I, Ruberti J, Sherwood JM, Dunlop IE, Paterson C, Török P, Overby DR. 2017. Brillouin microscopy, what is it really measuring? ArXiv 1711.03312. [Preprint].

Wu PJ, Kabakova IV, Ruberti JW, Sherwood JM, Dunlop IE, Paterson C, Török P, Overby DR. 2018. Water content, not stiffness, dominates Brillouin spectroscopy measurements in hydrated materials. Nature Methods **15**, 561–562.

Xi X, Kim SH, Tittmann B. 2015. Atomic force microscopy based nanoindentation study of onion abaxial epidermis walls in aqueous environment. Journal of Applied Physics **117**, 024703.

Xi X, Li X, Miyasaka C, Kropf M, Tittmann B. 2013. High frequency scanning acoustic microscopy as diagnostic tool in tissue science. Journal of Biotechnology & Biomaterials **3**, 1000160.

Yakubov GE, Bonilla MR, Chen H, Doblin MS, Bacic A, Gidley MJ, Stokes JR. 2016. Mapping nano-scale mechanical heterogeneity of primary plant cell walls. Journal of Experimental Botany **67**, 2799–2816.

Yanagisawa M, Desyatova AS, Belteton SA, Mallery EL, Turner JA, Szymanski DB. 2015. Patterning mechanisms of cytoskeletal and cell wall systems during leaf trichome morphogenesis. Nature Plants **1**, 15014.

Yi H, Puri VM. 2012. Architecture-based multiscale computational modeling of plant cell wall mechanics to examine the hydrogen-bonding hypothesis of the cell wall network structure model. Plant Physiology **160**, 1281–1292.

Yu Y, Jiang Z, Fei B, Wang G, Wang H. 2011. An improved microtensile technique for mechanical characterization of short plant fibers: a case study on bamboo fibers. Journal of Materials Science **46**, 739–746.

Yun SH, Chernyak D. 2018. Brillouin microscopy: assessing ocular tissue biomechanics. Current Opinion in Ophthalmology **29**, 299–305.

Zamil MS, Geitmann A. 2017. The middle lamella—more than a glue. Physical Biology **14**, 015004.

Zamil MS, Yi H, Haque MA, Puri VM. 2013. Characterizing microscale biological samples under tensile loading: stress–strain behavior of cell wall fragment of onion outer epidermis. American Journal of Botany **100**, 1105–1115.

Zamil MS, Yi H, Puri VM. 2015. The mechanical properties of plant cell walls soft material at the subcellular scale: the implications of water and of the intercellular boundaries. Journal of Materials Science **50**, 6608–6623.

Zamil MS, Yi H, Puri VM. 2017. A multiscale FEA framework for bridging cell-wall to tissue-scale mechanical properties: the contributions of middle lamella interface and cell shape. Journal of Materials Science **52**, 7947–7968.

Zerzour R, Kroeger J, Geitmann A. 2009. Polar growth in pollen tubes is associated with spatially confined dynamic changes in cell mechanical properties. Developmental Biology **334**, 437–446.

Zhang J, Fiore A, Yun SH, Kim H, Scarcelli G. 2016. Line-scanning Brillouin microscopy for rapid non-invasive mechanical imaging. Scientific Reports **6**, 35398.

Zhang T, Mahgsoudy-Louyeh S, Tittmann B, Cosgrove DJ. 2014. Visualization of the nanoscale pattern of recently-deposited cellulose microfibrils and matrix materials in never-dried primary walls of the onion epidermis. Cellulose **21**, 853–862.

Zhang T, Zheng Y, Cosgrove DJ. 2016. Spatial organization of cellulose microfibrils and matrix polysaccharides in primary plant cell walls as imaged by multichannel atomic force microscopy. The Plant Journal **85**, 179–192.

Zhao R, Boudou T, Wang WG, Chen CS, Reich DH. 2013. Decoupling cell and matrix mechanics in engineered microtissues using magnetically actuated microcantilevers. Advanced Materials **25**, 1699–1705.

Zheng Y-P, Choi A, Ling H, Huang Y-P. 2009. Simultaneous estimation of Poisson's ratio and Young's modulus using a single indentation: a finite element study. Measurement Science and Technology **20**, 045706.

Zou R, Xia Y, Liu S, Hu P, Hou W, Hu Q, Shan C. 2016. Isotropic and anisotropic elasticity and yielding of 3D printed material. Composites Part B: Engineering **99**, 506–513.

Zurlo G, Truskinovsky L. 2017. Printing non-Euclidean solids. Physical Review Letters **119**, 048001.